Am J Transl Res 2019;11(10):6462-6474
www.ajtr.org /ISSN:1943-8141/AJTR0097262

Original Article

The diagnostic and prognostic usage of circulating tumor DNA in operable hepatocellular carcinoma

Yan An[1*], Yanfang Guan[2,6*], Yaping Xu[2*], Yingxin Han[1*], Chi Wu[4], Chaohui Bao[1], Boping Zhou[3], Haiyan Wang[4], Mingxia Zhang[4], Weilong Liu[4], Lin Qiu[1], Zeguang Han[1,5], Yongsheng Chen[6], Xuefeng Xia[2], Jiayin Wang[6], Zhentian Liu[2], Wanqiu Huang[1], Xin Yi[2], Jian Huang[1,3,4,5]

[1]Key Laboratory of Systems Biomedicine (Ministry of Education) and Collaborative Innovation Center of Systems Biomedicine, Shanghai Center for Systems Biomedicine, Shanghai Jiao Tong University, Shanghai 200240, China; [2]Geneplus-Beijing, Beijing 102206, China; [3]Shenzhen People's Hospital, Second Clinical Medical College of Jinan University, Shenzhen 518109, China; [4]Shenzhen Key Laboratory of Infection and Immunity, Shenzhen Third People's Hospital, Guangdong Medical College, Shenzhen 518112, China; [5]Shanghai-MOST Key Laboratory for Disease and Health Genomics, Chinese National Human Genome at Shanghai, Shanghai 201203, China; [6]Department of Computer Science and Technology, School of Electronic and Information Engineering, Xi'an Jiaotong University, 28 West Xianning Road, Xi'an 710049, China. [*]Equal contributors.

Received May 9, 2019; Accepted August 9, 2019; Epub October 15, 2019; Published October 30, 2019

Abstract: Circulating tumor DNA (ctDNA) is a promising noninvasive biomarker for hepatocellular carcinoma (HCC). In this study, we aimed to assess the diagnostic and prognostic value of ctDNA in HCC. Twenty-six operable HCC, 10 hepatitis and 10 cirrhosis patients were enrolled in this study. Treatment-naïve blood samples were collected from all patients, nevertheless resected tissue and postoperative blood samples were only collected from HCC patients. A custom-designed sequencing panel covering 354 genes was used to identify somatic mutations. Collectively, we identified 139 somatic mutations from 25 HCC baseline plasma samples (96.2%). *TP53* (50.00%) was the most common mutant gene, and R249S was the most recurrent mutation (19.2%). Twenty-three patients (88.5%) carried at least one ctDNA mutation validated in matched tissue, and the driver mutations exhibited an advanced concordance than non-driver mutations (67.6% vs. 33.8%, $P = 0.0002$). For HCC patients, the number of mutations in ctDNA ($R^2 = 0.1682$, $P = 0.0375$), maximal variant allele frequency (VAF) in ctDNA ($R^2 = 0.4974$, $P < 0.0001$) and ctDNA concentration ($R^2 = 0.2676$, $P = 0.0068$) were linearly correlated with tumor size. Multiple circulating cell-free DNA (cfDNA) parameters could be used in differentiating malignant lesions from benign lesions, and the performance was no less than blood alpha-fetoprotein (AFP). HCC patients with detectable mutation in postoperative plasma had a poor DFS than those without (17.5 months vs. 6.7 months, HR = 7.655, $P < 0.0001$), and postoperative cfDNA status (HR = 10.293, $P < 0.0001$) was an independent risk factors for recurrence. In conclusion, ctDNA profiling is potentially valuable in differential diagnosis and prognostic evaluation of HCC.

Keywords: Circulating tumor DNA, next generation sequencing, hepatocellular carcinoma, differential diagnosis, prognostic evaluation

Introduction

Hepatocellular carcinoma (HCC) is the most common pathological subtype of primary liver cancer. It continues to be associated with a high mortality rate, at least partly because diagnosis usually occurs at advanced stage [1]. In 2012, 782,500 new cases and 745,500 deaths from liver cancer were reported worldwide, and approximately 50% of these cases and deaths occurred in China [2]. National Central Cancer Registry of China estimated that approximately 466,100 new cases and 422,100 deaths occurred throughout 2015 in China [3]. In current clinical practice, blood alpha-fetoprotein (AFP) level is widely used for tumor assessment during diagnosis, therapeutic evaluation, and surveillance. However, the sensitivity is far from satisfactory [4, 5]. Histological biopsy is the most powerful tool for diagnosis, but procedural risks and tumor heterogeneity have limited its applicability. Highly

sensitive, specific, and comprehensive methods are thereby required to optimize diagnosis and prognosis determination in HCC patients. Hepatitis and cirrhosis are the most common precancerous lesions of HCC and have been regarded as important risk factors of carcinogenesis [1, 6-9]. Revealing genomic discrepancy between precancerous lesions and HCC may provide molecular evidence to direct early intervention.

Circulating tumor DNA (ctDNA), which is derived from necrosis or apoptosis of vivo-cells, have been explored in the plasma of most solid tumors, including HCC [10]. ctDNA can contain tumor-specific genetic alterations and overcome the limitations of biopsies resulting from tumor heterogeneity [11-13]. The development of next generation sequencing (NGS) has facilitated the identification of genetic variants in various tumors and enables the detection and quantification of ctDNA. Noninvasive ctDNA sequencing via the NGS platform is a promising tool for genetic profiling of various tumors, which is potentially valuable for diagnosis and determining prognosis [14-16].

In this study, we examined tumor tissue and pre-/postoperative blood samples from 26 patients with HCC undergoing radical surgery, as well as blood samples from 10 patients with hepatitis and 10 with cirrhosis. Hybrid capture and panel-based sequencing were performed on all samples. Using integrated profiling, we evaluated the diagnostic and prognostic value of ctDNA in HCC patients.

Materials and methods

Clinical cohort

Twenty-six HCC, 10 hepatitis and 10 cirrhosis patients were enrolled in this study. All patients were treated at Shenzhen People's Hospital between August 22, 2013 and April 16, 2014. Clinicopathological data about demography and tumor histopathological results, such as TNM staging and cellular differentiation grade, were collected from each patient. This study was approved under the institutional review board of Shenzhen People's Hospital. All subjects provided informed, written consent before undergoing any study-related procedures. This study was performed in accordance with the Declaration of Helsinki.

Sample processing and DNA extraction

HCC tissue samples were collected during surgical resection. At least 10 ml of peripheral blood (PB) was collected using Streck tubes for all patients before they received any medical treatment, and for HCC patients except P009, further 10 ml of PB was collected after surgery (within 1 to 4 weeks). Within 72 h after collection, PB samples were centrifuged at 1,600 g for 10 min, then transferred to microcentrifuge tubes and centrifuged at 16,000 g for 10 min to remove cellular debris. PB lymphocytes (PBLs) located in the cell pellet generated during the first centrifugation were also separated and stored. Tissue, plasma, and PBLs were stored at -80°C prior to DNA extraction. PBL DNA and tissue DNA were extracted using the DNeasy Blood & Tissue Kit (Qiagen, Hilden, Germany), whereas circulating cell-free DNA (cfDNA) was isolated from 0.6-1.8 mL plasma using QIAamp Circulating Nucleic Acid Kit (Qiagen). The Qubit fluorometer (Invitrogen, Carlsbad, CA, USA) dsDNA HS kit was used to determine the DNA concentration, and the size of cfDNA fragments was assessed using the Agilent 2100 BioAnalyzer and DNA HS kit (Agilent Technologies, Santa Clara, CA, USA).

Sequencing library construction and target enrichment

Before library construction, 1 μg of tissue DNA and PBL DNA were cut into 200-250 bp fragments with a Covaris S2 instrument (Woburn, MA, USA). Indexed Illumina NGS libraries were prepared from tissue, PBL germline, and circulating DNA using the KAPA Library Preparation Kit (Kapa Biosystems, Boston, MA, USA). For cfDNA, after end repairing and A-tailing, well-designed adapters with unique identifiers were ligated to both ends of the double-stranded cfDNA fragments, in order for the cluster and error correction. A custom SeqCap EZ Library (Roche NimbleGen, Madison, WI, USA) was used during the process of target enrichment. PCR cycles were performed to generate enough quantity of fragments prior to hybridization. Capture hybridization was performed with a specific gene panel, according to the manufacturer's protocol. Amplification of the captured DNA fragments was conducted after hybrid selection and then pooled to several multiplexed libraries. Additional detailed information regarding library preparation and tar-

get enrichment was described in a previous article [17].

Capture panel design

Considering the known genomic heterogeneity of HCC, a comprehensive capture probe was designed based on cancer genomic data from COSMIC (http://cancer.sanger.ac.uk/cosmic). Among 719 genes registered in the COSMIC database (v84), we first eliminated those altered solely in hematological malignancies. We then screened frequently variable genomic regions presenting in not only HCC but also in other common malignancies to generate the prototype of our capture panel. Entire exons of certain notable oncogenes and suppressor genes, such as *TP53*, *RAS*, and *EGFR*, were then added. Data from our own sequencing and TCGA (https://cancergenome.nih.gov/) were also taken into consideration. From the above efforts, we ultimately generated a specific capture panel covering 354 genes (Table S1).

Next generation sequencing

Sequencing was performed by Illumina 2 × 75 bp paired-end sequencing using Illumina HiSeq 3000 and NextSeq 500 instruments (Illumina, San Diego, CA, USA). The TruSeq PE Cluster Generation Kit V3 and TruSeq SBS Kit V3 (Illumina, San Diego, CA, USA) were used according to the manufacturer's recommendations. The preset amount of data was 1, 2, or 15 Gb for PBL DNA, tissue DNA, or cfDNA, respectively. Additional detailed information about NGS was described in a previous article [17].

Raw data processing

After adaptor sequences, sequences with more than 50% low-quality base reads, or those with more than 50% N bases, together with their mate pairs were removed, remaining reads were mapped to the reference human genome (hg19) using the Burrows-Wheel Aligner (http://bio-bwa.sourceforge.net/) with default parameters. Picard's Mark Duplicates tool (https://software.broadinstitute.org/gatk/documentation/tooldocs/4.0.3.0/picard_sam_markduplicates_MarkDuplicates.php) was used to identify and mark duplicate reads for tumor and germline DNA data and clustered cfDNA reads according to UID and position of the template fragments. The average depth was 724.3 ± 180.1 × for 26 tissue samples, and 1899 ± 417.1 × for 71 plasma samples (Table S2). Mistakes introduced by PCR or sequencing procedures were corrected according to clustered reads. Local realignment and base quality recalibration were performed using The Gene Analysis Toolkit (https://www.broadinstitute.org/gatk/).

Sequence data analysis

Somatic single-nucleotide variations (SNVs) and insertions or deletions of small fragments (Indels) were called by MuTect algorithm (https://software.broadinstitute.org/gatk/documentation/tooldocs/3.8-0/org_broadinstitute_gatk_tools_walkers_cancer_m2_MuTect2.php). PBL sequencing data were used to filter out germline mutations. The filter criteria included: (1) variants supported by fewer than five high-quality reads (base quality ≥ 30, mapping quality ≥ 30) were filtered ; (2) variants were filtered as cross-contamination if present in > 1% samples in custom single nucleotide polymorphism (SNP) databases (dbsnp, https://www.ncbi.nlm.nih.gov/projects/SNP/; 1000G, https://www.1000genomes.org/; ESP6500, https://evs.gs.washington.edu/; ExAC, http://exac.broadinstitute.org/) and self-built SNP database; (3) synonymous mutations; (4) variants detected in matched blood lymphocytes. The variant allele frequency (VAF) indicated the percentage of mutant reads in total reads. An online tool WebGestalt (http://www.webgestalt.org) were used for gene enrichment analysis.

ctDNA quantification and quantitative variation of cfDNA or ctDNA concentration

The calculation of ctDNA concentration: ctDNA concentration (ng/ml) = Maximal VAF × cfDNA concentration (ng/ml).

The calculation of quantitative variation: [Postoperative DNA concentration (ng/ml) - Baseline DNA concentration (ng/ml)]/Baseline DNA concentration (ng/ml).

Statistical analysis

Mann-Whitney U-test was used to estimate differences between two groups, and one-way ANOVA was utilized to assess significant differences among three or more groups. The difference between proportions of two groups was assessed using Chi-square test. These tests, as well as descriptive statistics, were performed using SPSS 22.0 (IBM, Armonk, NY, USA).

Table 1. The association between clinicopathologic characteristics and cfDNA parameters

Characteristics	N (%) Total = 26	Mutation number in cfDNA		Maximal VAF in cfDNA (%)		cfDNA concentration (ng/ml)		Mutant cfDNA concentration (ng/ml)	
		Mean ± SD	*p*	Mean ± SD	*p*	Mean ± SD	*p*	Mean ± SD	*p*
Age, years									
≤ 50	12 (46.2%)	4.7 ± 4.6	0.437	3.6 ± 5.0	0.453	39.3 ± 35.7	0.595	1.1 ± 1.5	0.296
> 50	14 (53.8%)	5.9 ± 3.5		6.2 ± 10.9		52.5 ± 78.1		2.4 ± 4.4	
Gender									
Male	23 (88.5%)	5.3 ± 4.2	0.887	5.3 ± 9.2	0.596	49.6 ± 64.8	0.483	2.0 ± 3.6	0.511
Female	3 (11.5%)	5.7 ± 2.5		2.4 ± 1.7		22.4 ± 2.5		0.6 ± 0.4	
HBV infection									
Positive	25 (96.2%)	5.3 ± 4.1	0.872	5.1 ± 8.8	0.777	46.9 ± 62.7	0.865	1.8 ± 3.5	0.794
Negative	1 (3.8%)	6.0		2.5		35.9		0.9	
AFP									
≤ 400 ng/ml	16 (61.5%)	4.8 ± 3.5	0.350	4.4 ± 9.6	0.677	53.9 ± 77.0	0.448	1.4 ± 3.0	0.506
> 400 ng/ml	10 (38.5%)	6.3 ± 4.8		5.9 ± 7.4		34.6 ± 19.0		2.4 ± 4.1	
Clinical stage									
I	20 (76.9%)	4.8 ± 3.2	0.357	4.2 ± 8.8	0.402	47.8 ± 67.6	0.844	1.3 ± 2.7	0.164
II/III	6 (23.1%)	7.3 ± 6.1		7.6 ± 9.2		42.0 ± 21.4		3.5 ± 5.1	
Edmondson grade									
I/II	21 (80.8%)	5.6 ± 4.2	0.490	4.9 ± 9.1	0.908	48.8 ± 68.1	0.696	1.8 ± 3.7	0.932
III	5 (19.2%)	4.2 ± 3.1		5.4 ± 7.0		36.5 ± 16.4		1.7 ± 2.2	
PVTT									
Positive	3 (11.5%)	2.7 ± 2.9	0.228	7.6 ± 9.0	0.587	29.6 ± 2.3	0.624	2.3 ± 2.8	0.773
Negative	23 (88.5%)	5.7 ± 4.1		4.6 ± 8.8		48.6 ± 65.2		1.7 ± 3.5	
Associated with cirrhosis									
Positive	19 (73.1%)	4.6 ± 3.0	0.254	4.3 ± 6.6	0.552	51.0 ± 71.0	0.540	1.7 ± 3.2	0.800
Negative	7 (26.9%)	7.4 ± 5.8		6.7 ± 13.3		33.9 ± 19.3		2.1 ± 4.2	
Largest tumor diameter									
≤ 5 cm	16 (61.5%)	4.1 ± 3.2	0.048*	2.7 ± 5.2	0.085	29.4 ± 14.2	0.072	1.2 ± 3.2	0.245
> 5 cm	10 (38.5%)	7.3 ± 4.6		8.7 ± 11.8		73.7 ± 93.8		2.8 ± 3.6	
Focal									
Single	22 (84.6%)	4.4 ± 3.2	0.003*	4.0 ± 8.2	0.199	59.0 ± 87.7	0.816	6.0 ± 24.5	0.930
Multiple	4 (15.4%)	10.5 ± 4.7		10.2 ± 10.5		48.5 ± 24.3		4.9 ± 6.0	

Abbreviations: AFP, alpha fetal protein; HBV, hepatitis B virus; HCC, hepatocellular carcinoma; PVTT, portal vein tumor thrombus. *Statistical significance.

Receiver operating characteristic (ROC) analysis was performed using GraphPad Prism 7 (GraphPad Software, La Jolla, CA, USA). We also used Spearman correlation analysis to assess correlations between experimental parameters using GraphPad Prism 7 (GraphPad Software). Kaplan-Meier and COX survival analysis (SPSS 22.0, IBM) was used to compare DFS between subgroups. Results were considered statistically significant when the *p* value was less than 0.05.

Results

Description of study cohort

The median diagnostic age of enrolled HCC patients was 51 (ranged from 27-86). Male subjects accounted for the majority (23/26, 88.5%). Almost all (25/26, 96.2%) had a history of hepatitis B virus (HBV) infection, and none had ever been infected with hepatitis C virus (HCV). Twenty patients (76.9%) had clinical stage I disease, whereas 15.4% (4/26) and 7.7% (2/26) had stage II and III disease, respectively. According to Edmondson grade system, the majority (21/26, 80.8%) was identified as grade I/II cellular differentiation. Portal vein tumor thrombus (PVTT) was detected in three patients (11.5%). Meanwhile concomitant cirrhosis existed in 19 patients (73.1%). The largest tumor diameter (LTD) was less than or equal to 5 cm in 61.5% (16/26) of patients with HCC. Only four patients (15.4%) had multiple malignant foci. Abnormal elevation of AFP (> 400 ng/ml) was seen in 10 patients (38.5%) (**Table 1**).

As a contrast, the median diagnostic ages of hepatitis and cirrhosis patients were 32 (ranged from 18-50) and 48.5 (ranged from 31-76),

respectively. Most of hepatitis (7/10, 70%) and all of cirrhosis patients were male. Only two cirrhosis patients were not infected with HBV. None was in AFP > 400 ng/ml, and the range was 2.9-89.5 ng/ml and 1.5-46.9 ng/ml for hepatitis and cirrhosis patients (Table S3).

Genomic landscape revealed by ctDNA profiling and mutational validation via matched tumor tissue sequencing

A total of 139 somatic mutations involving 93 genes were detected in 25 baseline (preoperative) plasma samples (96.2%), with a median of 5 (ranged from 0 to 17) per sample. *TP53* (13/26, 50.00%) was the most common mutant gene. Besides, *AXIN1* (3/26, 11.54%), *BCOR* (3/26, 11.54%), *CTNNB1* (3/26, 11.54%), *FANCE* (3/26, 11.54%), *FANCM* (3/26, 11.54%), and *NCOR1* (3/26, 11.54%) were mutated in over two plasma samples (**Figure 1A**).

Subsequently, these mutations detected in plasma ctDNA were explored in matched tumor tissue. Within 139 mutations detected in ctDNA, 69 (49.6%) could be validated in paired tumor DNA (tDNA), and the other 70 mutations (50.4%) were private in plasma samples (0 to 15 for each patient). In addition, 28 mutations were private in tDNA (**Figures 1B**, S1, S2). At least one overlapping mutation could be detected in 23 patients (88.5%). Furthermore, all ctDNA mutations could be validated in matched tDNA for seven patients (26.9%) (Figure S2).

Next, we selected nine presumptive driver genes for HCC, including *TP53, AXIN1, CTNNB1, CDKN2A, ARIN1A, ARID2, SMARCA4, KEAP1* and *NFE2L2* [18] and further explored their concordance between ctDNA and tDNA. A total of 37 driver events were identified in 23 patients (88.5%), and three patients (11.5%) lacked conventional driver events in both ctDNA and tDNA. Within these driver events, 25 (67.6%) were shared in paired ctDNA and tDNA, whereas three (8.1%) were plasma-private and nine (24.3%) were tissue-private (**Figure 1C**). Interestingly, the driver mutations exhibited an advanced concordance than non-driver mutations (25/37, 67.6% versus 44/130, 33.8%, Chi-square *p* value = 0.0002), indicating that it was more possible to trace driver than non-driver mutations in ctDNA (Figure S3).

Mutant *TP53* was detected in 69.23% (18/26) patients with HCC in either ctDNA or tDNA (Figure S1), and R249S could be detected in five (19.2%) ctDNA and six (23.1%) tDNA (Figure S4A). For comparison, within 373 profiled HCC tissue from TCGA, 115 (30.83%) samples had a *TP53* mutation, of which 11 (2.9%) contained R249S (Figure S4B). This variant was the most recurrent in both TCGA and our cohort, but the population frequency in our cohort was much higher than that in TCGA (23.1% versus 2.9%, Chi-square *p* value = 0.0001).

Correlation between clinicopathologic factors and ctDNA mutations

In this section, we compared several cfDNA parameters, including number of mutations, maximal VAF, cfDNA concentration and ctDNA concentration, between patients grouped by different clinicopathologic factors. The results presented that most of these factors were not related to cfDNA parameters. However, the number of mutations in ctDNA was significantly higher in patients with the LTD > 5 cm or multiple malignant focuses than in those with LTD ≤ 5 cm ($P = 0.048$) or single focuses ($P = 0.003$) (**Table 1**). Besides, we found that although the discrepancy of other parameters between two groups with LTD > or ≤ 5 cm did not reach statistical significance, the patients with LTD > 5 cm tended to suggest higher parameters than those with LTD ≤ 5 cm (**Table 1**). Therefore we next performed a linear regression analysis to further explore the correlation between these parameters and LTD. Results showed that the number of mutation ($R^2 = 0.1682$, $P = 0.0375$), maximal VAF ($R^2 = 0.4974$, $P < 0.0001$) and ctDNA concentration ($R^2 = 0.2676$, $P = 0.0068$) presented modest but significant linear dependence with LTD (**Figure 2**). AFP was also assessed, but no linear correlation with LTD was found ($R^2 = 0.0121$, $P = 0.5927$, **Table 1**).

Molecular differentiation between hepatitis/cirrhosis and HCC via quantitative analysis of cfDNA

In order to assess the capacity of cfDNA in differential diagnosis between malignant and benign classification, we performed the same sequencing and analysis strategies for plasma cfDNA from 10 hepatitis and 10 cirrhosis patients. Overall, we identified 21 somatic mutations from two hepatitis and six cirrhosis patients. Most notably, both *ARID1B* and *ARID2* mutations were identified in two cirrhosis pa-

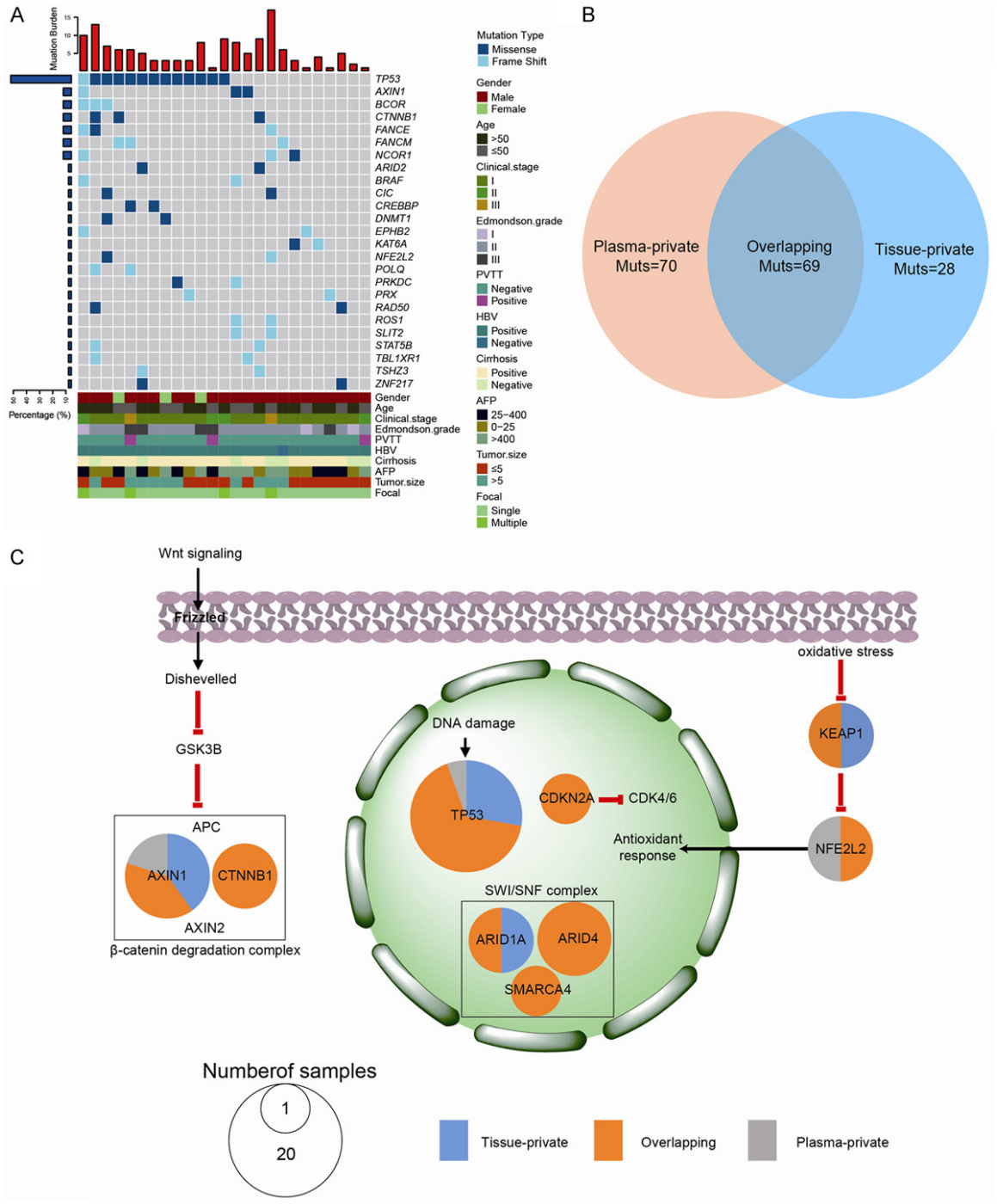

Figure 1. Genomic landscape of cfDNA from patients with hepatocellular carcinoma. A. Heatmap illustrating aromatic mutations detected in baseline plasma. Only genes that were mutated over two samples are shown. The lower bar charts present the clinicopathologic characteristics of patients, and the upper bar charts represent the number of mutations in each patient. The left bars show the frequencies of specific altered genes in the total cohort. B. Venn diagram providing an overview of detectable mutations in tumor tissue and baseline plasma. C. Concordance of presumptive driver genes of HCC. The subcellular localization of each transcript is shown. The size of circle indicates the patient number with specific mutant genes. The fractions of overlapping, tissue-private and plasma-private mutations in different genes are represented by the orange, blue and grey parts, respectively.

tients (Figure S5). Subsequently, the cfDNA parameters and AFP level were compared between hepatitis/cirrhosis and HCC patients. The AFP (P = 0.0368) and cfDNA concentration (P

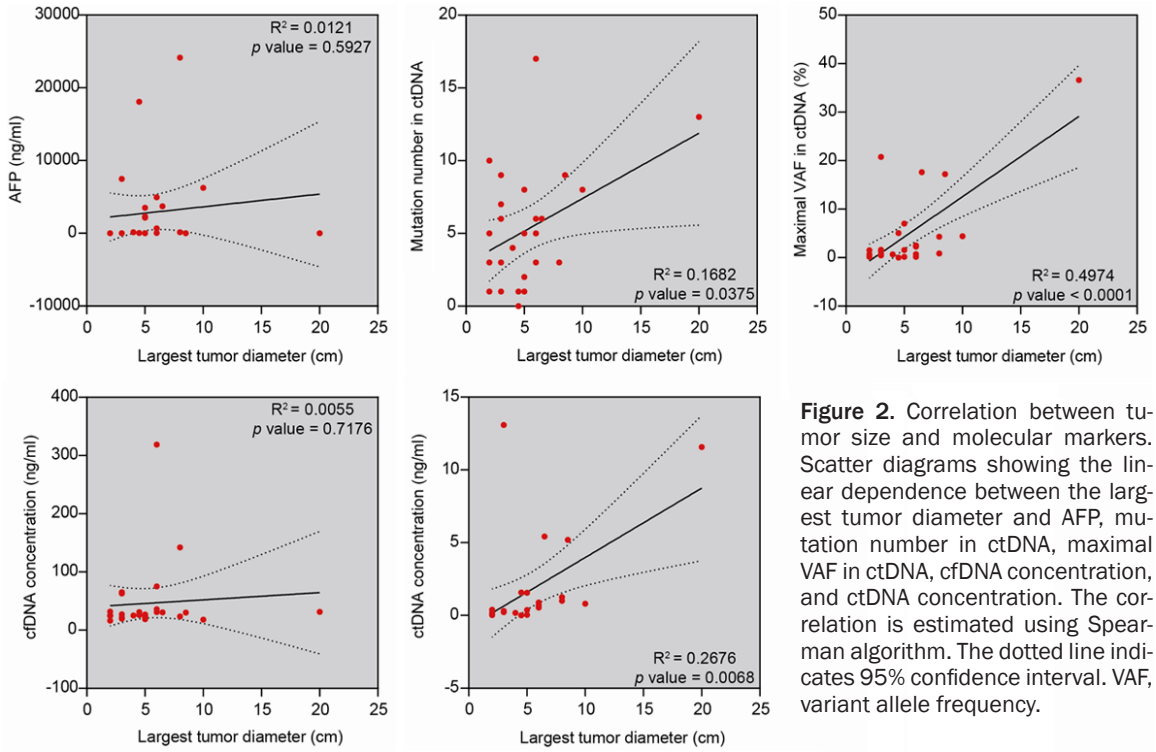

Figure 2. Correlation between tumor size and molecular markers. Scatter diagrams showing the linear dependence between the largest tumor diameter and AFP, mutation number in ctDNA, maximal VAF in ctDNA, cfDNA concentration, and ctDNA concentration. The correlation is estimated using Spearman algorithm. The dotted line indicates 95% confidence interval. VAF, variant allele frequency.

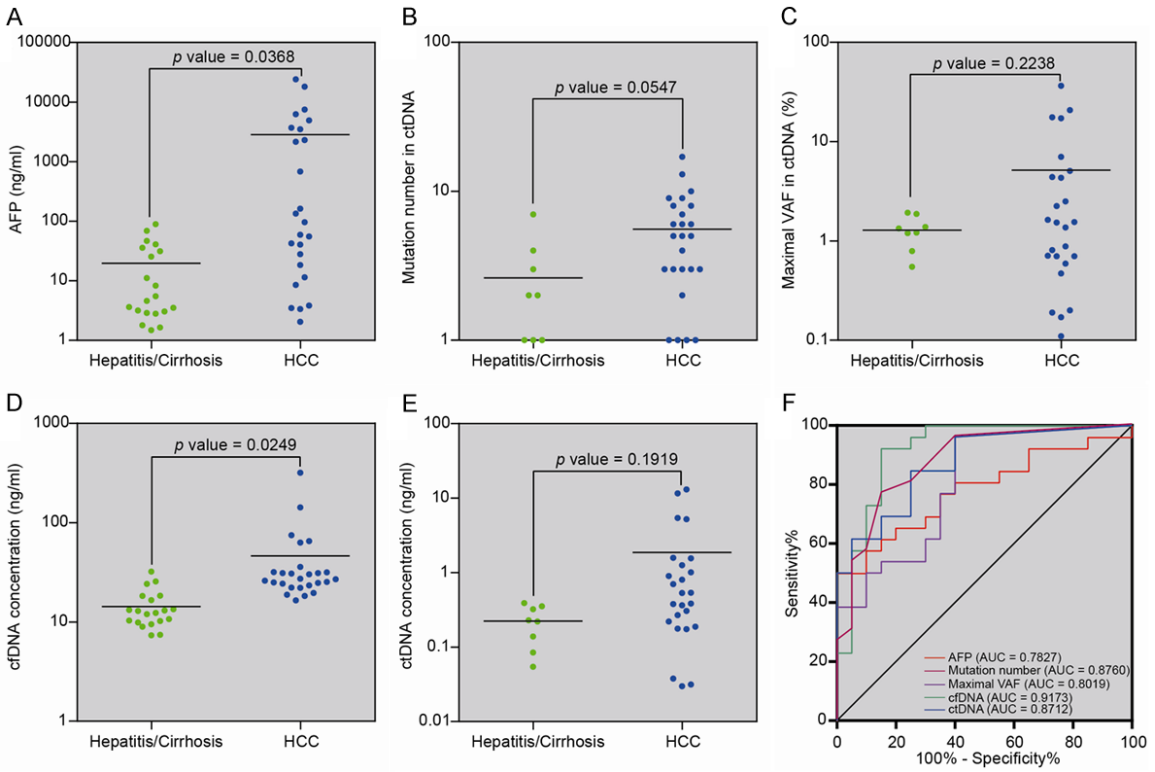

Figure 3. Discrepancy of blood biomarkers between hepatitis/cirrhosis and HCC. Comparison of AFP (A), mutation number in ctDNA (B), maximal VAF in ctDNA (C), cfDNA concentration (D), and ctDNA concentration (E) between hepatitis/cirrhosis and HCC. The horizontal line represents the mean of each group. *P* value is calculated via Mann-Whitney U-test. (F) ROC curve distinguishing HCC from hepatitis/cirrhosis via multiple blood molecular markers. Each broken line represents the performance of one specific marker. VAF, variant allele frequency.

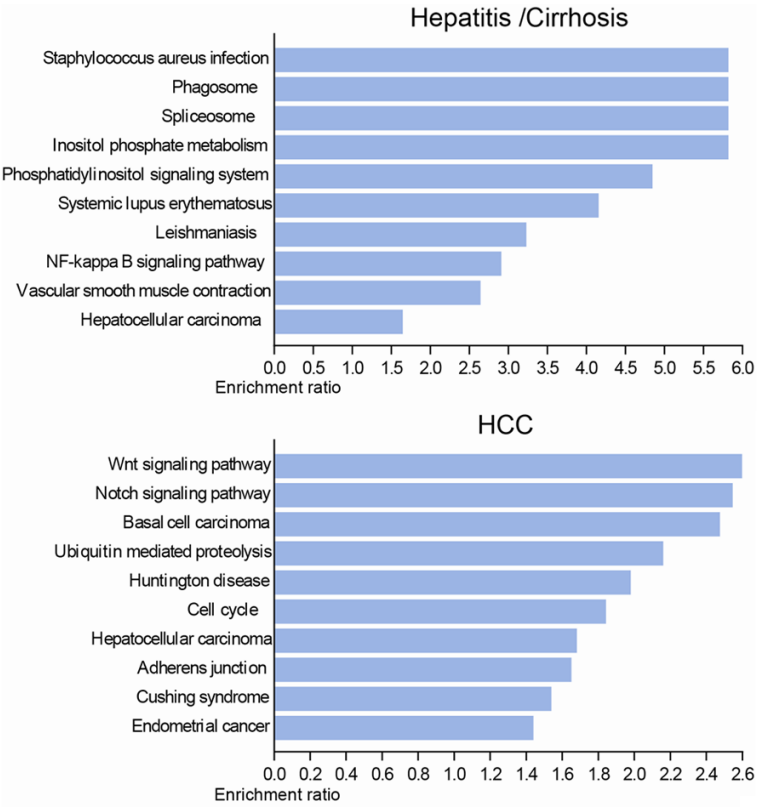

Figure 4. Gene enrichment analysis for genomic aberrations of cfDNA. The upper and lower bar charts indicate the molecular pathways affected by hepatitis/cirrhosis and HCC mutations, respectively. Only top 10 pathways are shown and ranked in order of enrichment ratio.

= 0.0249) of HCC patients were significantly higher than those of hepatitis/cirrhosis patients (**Figure 3A**, **3B**). The number of mutations, maximal VAF and ctDNA concentration of HCC patients also tended to exceed those of hepatitis/cirrhosis patients, but the discrepancy did not reach significance level partly due to the small population of hepatitis/cirrhosis patients with somatic mutations in cfDNA (**Figure 3C-E**). Thus, we further explored the differentiating capacity of cfDNA using ROC analysis, and results showed that all cfDNA parameters performed equally to or better than AFP in differential diagnosis (**Figure 3F**).

Pathway enrichment was executed for cfDNA mutations in hepatitis/cirrhosis or HCC plasma. Based on the enrichment ratio, the pathways that hepatitis/cirrhosis mutations most significantly enriched in were Staphylococcus aureus infection, Phagosome, Spliceosome and Inositol phosphate metabolism. However, Wnt and Notch signaling pathways were most significantly influenced by HCC mutations, indicating the critical roles of these two pathways in the genesis and development of HCC (**Figure 4**).

Clearance of ctDNA associated with postoperative survival of HCC

Postoperative blood sample were collected from 25 HCC patients, and the quantitative variation of cfDNA and ctDNA were drawn for each patient. As shown in **Figure 5A**, the cfDNA concentration rose postoperatively in 18 patients (72%), while only two patients (8%) experienced postoperative rises of ctDNA concentration. We defined the patients without somatic mutations in postoperative blood as the total clearance cohort and the others as the mutational residual cohort. All of patients in the mutational residual cohort (12/12) experienced in-situ or distant recurrence postoperatively, while only 30.8% (4/13) of patients in the total clearance cohort experienced recurrence events (Chi-square $P = 0.0005$) (**Table 2**). According to Kaplan-Meier survival analysis, the mutational residual cohort had a significantly poor DFS than the total clearance cohort (median: 8.3 months versus unreached, log-rank HR = 7.655, $P < 0.0001$, **Figure 5B**). Even in the mutational residual cohort, if we grouped these patients based on the median of quantitative variation, those with high clearance rates (-59.3% to -98.5%) suggested an improved DFS than the others (265.4% to -42.2%) (median: 17.5 months versus 6.7 months, log-rank HR = 3.164, $P = 0.0195$, **Figure 5C**). However, only PVTT among involved clinicopathologic factors was significantly associated with DFS (median: 8.2 months versus 25.2 months, log-rank HR = 4.036, $P = 0.0413$, Figure S6).

Next, we enrolled clinicopathologic factors with log-rank HR > 2, as well as ctDNA status, to perform multivariable COX regression analysis.

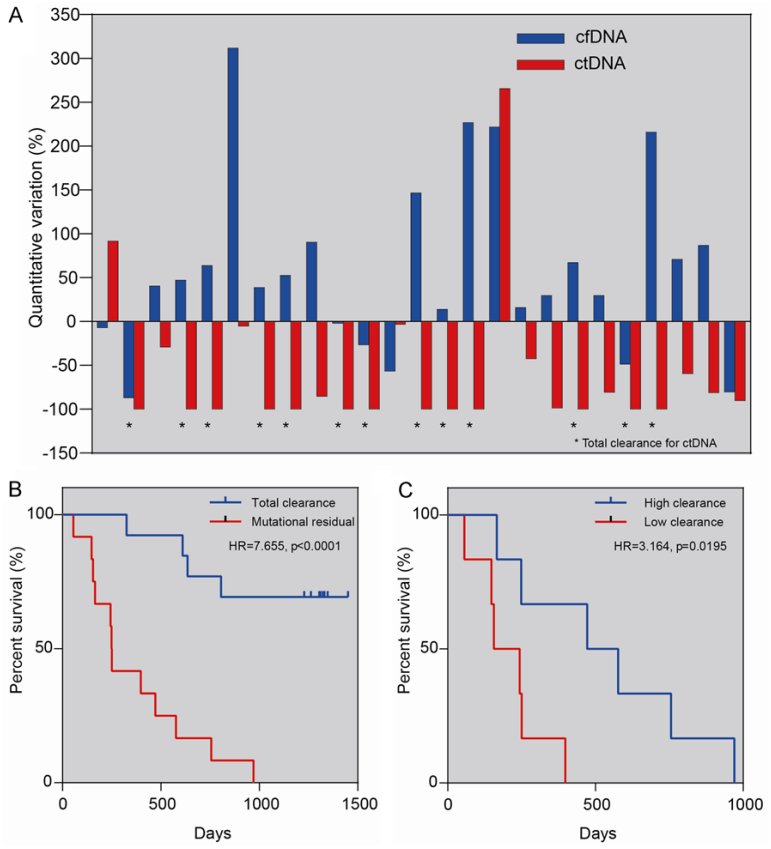

Figure 5. Prognostic evaluation of postoperative cfDNA status. A. The quantitative variation of cfDNA and ctDNA concentration between baseline plasma and postoperative plasma. The adjacent blue and red bars represent the change of cfDNA and ctDNA concentration for the same patient. The calculation of ctDNA (mutant cfDNA) concentration: ctDNA concentration (ng/ml) = Maximal VAF × cfDNA concentration (ng/ml). The calculation of quantitative variation: [Postoperative DNA concentration (ng/ml) - Baseline DNA concentration (ng/ml)]/Baseline DNA concentration (ng/ml). The asterisks indicate patients without detectable mutation in postoperative blood. B. Patients with and without detectable mutation in postoperative blood demonstrate differentiated disease-free survival. C. Patients with high and low clearance rate of ctDNA concentration demonstrate differentiated disease-free survival. The high and low clearance rate is determined by the median. Kaplan-Meier analysis is used to evaluate the survival differences.

Results showed that the postoperative clearance of ctDNA (HR = 10.293, $P < 0.0001$) and PVTT status (HR = 6.930, $P = 0.030$) were the independent factors associated with DFS of HCC patients (**Table 2**).

Discussion

The use of liquid biopsy and ctDNA profiling has been explored in multiple solid tumors [19]. Herein we reported a study using panel-based NGS to explore the diagnostic and prognostic value of ctDNA for HCC patients. As a result, almost all of HCC patients (96.2%) had ctDNA mutations which could be validated in matched tumor tissue, and there was a modest linear correlation between cfDNA parameters and clinical tumor burden measured by LTD. Besides, ctDNA profiling might be useful in differential diagnosis of benign and malignant liver lesions, and the postoperative status of cfDNA was associated with postoperative DFS for HCC patients.

AFP is the routine screening and diagnostic biomarker for HCC. However, AFP level also elevates in many physiological and pathological phenomena, suggesting it not a specific biomarker for HCC [20, 21]. Thus, diagnostic biomarkers with high sensitivity and specificity are urgently needed. As shown in this study, several cfDNA parameters were quite different between hepatitis/cirrhosis and HCC, and the differential performance was equal to or exceed that of AFP. Furthermore, the molecular functions influenced by HCC mutations appeared to be diverse from those influenced by hepatitis/cirrhosis mutations, and for HCC plasma, the Wnt and Notch signaling pathways were most significantly enriched in. However, these markers also lack the specificity for HCC. For instance, Wnt signaling was first identified for its role in carcinogenesis, and many mutations involved in this pathway were also identified in breast and prostate cancer [22]. Thus, it is necessary to combine HCC-specific mutations for precise screening and diagnosis of HCC. This study suggests that *TP53* R249S is the most common mutation. Actually, R249S is strongly associated with Aflatoxin-induced HCC [23, 24], and the higher population frequency in this study over that in TCGA may indicate the inter-ethnic dietary difference between Chinese and Caucasian. Moreover, the detection sensitivity

Table 2. Cox regression analysis about risk factors for postoperative recurrence

Factors	N, Recurrence/ Total	Median DFS, months	Cox *p* value
Clinical stage			
I	12/20	26.0	0.278
II/III	4/5	8.3	
Edmondson grade			
I/II	13/21	25.2	0.844
III	3/4	9.4	
PVTT			
Positive	2/2	8.2	0.030*
Negative	14/23	25.2	
Associated with cirrhosis			
Positive	13/18	19.8	0.691
Negative	3/7	Unreached	
Focal			
Single	13/21	21.2	0.652
Multiple	3/4	6.9	
Mutant cfDNA			
Total clearance	4/13	Unreached	< 0.001*
Mutational residual	12/12	8.3	

Abbreviations: DFS, disease-free survival; PVTT, portal vein tumor thrombus. *Statistical significance.

of ctDNA for this mutation is passable (5/6, 83.3%), suggesting it a promising biomarker for Chinese HCC screening and diagnosis via liquid biopsy. A critical issue is that the population coverage of R249S is just about 20%. Therefore it is needed to reveal more HCC-specific mutational markers to further improve the diagnostic performance.

An innovation of this study is that we also profiled cfDNA for hepatitis and cirrhosis patients and identified somatic mutations in some of them. It is remarkable that two cirrhosis patients had both mutant *ARID1B* and *ARID2*, both of which are associated with packaging of the SWI/SNF complex. The mammalian SWI/SNF (mSWI/SNF) complex performs a tumor suppressive function in many malignancies [25]. Several studies revealed that multiple subunits of the mSWI/SNF complex are frequently mutated in solid tumors [26-30]. A meta-analysis showed that SWI/SNF complex genes are mutated in approximately 20% of human malignancies [31]. Based on our finding, it seems that the existence of aberrant SWI/SNF complex is a critical event in both benign and malignant lesions of liver, for those several genes related with SWI/SNF complex, including *ARID1A*, *ARID2* and *SMARCA4*, also mutated in HCC tissue and plasma. The collection of sequential blood samples from precancerous lesions to tumorigenesis in the same HCC patient is in our plan, in order to further clarify the role of aberrant SWI/SNF complex in the genesis and development of HCC.

For ctDNA-based liquid biopsy, one of the greatest concerns is the concordance between ctDNA and tDNA. In this study, although most of presumptive driver mutations in plasma could be validated in matched tissue, a considerable number of ctDNA mutations were not traced from tDNA. Several factors may contribute to the incomplete overlap between mutant spectra of ctDNA and tDNA. Firstly, spatial heterogeneity can lead to sampling bias and thus incomplete profile of tumor genomic [32-36]. Secondly, variants related to clonal hematopoiesis, such as mutant *DNMT3A*, *JAK2,* and *TET2*, which are specific to plasma, can interfere with the detection of tumor-derived mutations in cfDNA [37, 38]. Indeed, such incomplete overlap is the greatest barrier for clinical application of ctDNA. Therefore, a large-scale ctDNA database including multiple cancer types and healthy people and standardized comparison between multi-region tissue and plasma are necessary in future ctDNA-related studies.

Minimal residual disease (MRD) is considered an important factor generating postoperative recurrence, and ctDNA detection has been proven an effective method for detecting MRD in colorectal cancer [39], lung cancer [40] and breast cancer [41]. Similarly, in HCC, the prognosis was significantly worse for patients with ctDNA in postoperative blood than those without. Even in patients with postoperative mutational residual, the DFS of those with high clearance rates was significantly improved than that of the others. Both qualitative and quantitative analysis demonstrate that ctDNA is a potential marker to predict postoperative recurrence and survival for HCC patients. Considering our finding that several cfDNA parameters presented a modest but significant linear dependence with LTD, we assume that ctDNA could be also used

in postoperative surveillance of HCC, which we will verify in the future study.

Some limitations persist in this study. Firstly and the most importantly, the study population is small, inducing the statistical non-significance of several analysis and inability of subset analysis. Besides, blood samples from healthy subjects are absent in this study, so we could not estimate the specificity of mutational detection in ctDNA. However, our results are still beneficial to promoting a standardized sequencing process and a rigorous strategy for identifying HCC-related mutations. In addition, we also plan to create a validation set to verify our findings in this study.

In conclusion, we present for the first time a preliminary framework of integrating ctDNA profiling into the management of operable HCC. Our results demonstrate the diagnostic and prognostic utility of ctDNA in HCC patients. Through integrated analysis of cfDNA from hepatitis/cirrhosis and HCC, we identified molecular discrepancy, which may be useful in the differential diagnosis between benign and malignant lesions of liver. Furthermore, postoperative ctDNA status was valuable in evaluating the recurrence risk. Combining our results with other novel efforts, such as evaluation of methylation or circulating tumor cells [42, 43], is a promising strategy for improving the clinical management of HCC patients.

Acknowledgements

The authors would like to acknowledge all department colleagues for their constructive suggestions. This work was supported by grants from the China National Key Projects for Infectious Disease (2017ZX10203207), the Chinese National Key Program on Basic Research (2014CB965002), the National Natural Science Foundation of China (81272306, 81472639 and 81872274), and the Shanghai Commission for Science and Technology (15431902900).

Disclosure of conflict of interest

None.

Address correspondence to: Jian Huang and Wanqiu Huang, Key Laboratory of Systems Biomedicine (Ministry of Education) and Collaborative Innovation Center of Systems Biomedicine, Shanghai Center for Systems Biomedicine, Shanghai Jiao Tong University, No. 800 Building, Dongchuan Road, Shanghai 200240, China. Tel: 0086139-1764-0385; E-mail: jianhuang@sjtu.edu.cn (JH); Tel: 86+21-34205108; E-mail: wanqiuhuang@sjtu.edu.cn (WQH); Dr. Xin Yi, Geneplus-Beijing, 9th Floor, No. 6 Building, Peking University Medical Industrial Park, Zhongguancun Life Science Park, Beijing 102206, China. Tel: 0086186-8893-7120; E-mail: yix@geneplus.org.cn

References

[1] El-Serag HB and Rudolph KL. Hepatocellular carcinoma: epidemiology and molecular carcinogenesis. Gastroenterology 2007; 132: 2557-2576.

[2] Torre LA, Bray F, Siegel RL, Ferlay J, Lortet-Tieulent J and Jemal A. Global cancer statistics, 2012. CA Cancer J Clin 2015; 65: 87-108.

[3] Chen W, Zheng R, Baade PD, Zhang S, Zeng H, Bray F, Jemal A, Yu XQ and He J. Cancer statistics in China, 2015. CA Cancer J Clin 2016; 66: 115-132.

[4] Tang JC, Feng YL, Guo T, Xie AY and Cai XJ. Circulating tumor DNA in hepatocellular carcinoma: trends and challenges. Cell Biosci 2016; 6: 32.

[5] Attwa MH and El-Etreby SA. Guide for diagnosis and treatment of hepatocellular carcinoma. World J Hepatol 2015; 7: 1632-1651.

[6] Kondo Y and Shimosegawa T. Significant roles of regulatory T cells and myeloid derived suppressor cells in hepatitis B virus persistent infection and hepatitis B virus-related HCCs. Int J Mol Sci 2015; 16: 3307-3322.

[7] Cho JY, Paik YH, Sohn W, Cho HC, Gwak GY, Choi MS, Lee JH, Koh KC, Paik SW and Yoo BC. Patients with chronic hepatitis B treated with oral antiviral therapy retain a higher risk for HCC compared with patients with inactive stage disease. Gut 2014; 63: 1943-1950.

[8] Pinzani M, Rosselli M and Zuckermann M. Liver cirrhosis. Best Pract Res Clin Gastroenterol 2011; 25: 281-290.

[9] Beste LA, Leipertz SL, Green PK, Dominitz JA, Ross D and Ioannou GN. Trends in burden of cirrhosis and hepatocellular carcinoma by underlying liver disease in US veterans, 2001-2013. Gastroenterology 2015; 149: 1471-1482, e1475; quiz e1417-1478.

[10] Wan JCM, Massie C, Garcia-Corbacho J, Mouliere F, Brenton JD, Caldas C, Pacey S, Baird R and Rosenfeld N. Liquid biopsies come of age: towards implementation of circulating tumour DNA. Nat Rev Cancer 2017; 17: 223-238.

[11] Bettegowda C, Sausen M, Leary RJ, Kinde I, Wang Y, Agrawal N, Bartlett BR, Wang H, Luber B, Alani RM, Antonarakis ES, Azad NS, Bardelli A, Brem H, Cameron JL, Lee CC, Fecher LA, Gallia GL, Gibbs P, Le D, Giuntoli RL, Goggins M, Hogarty MD, Holdhoff M, Hong SM, Jiao Y, Juhl HH, Kim JJ, Siravegna G, Laheru DA, Lauricella C, Lim M, Lipson EJ, Marie SK, Netto GJ, Oliner KS, Olivi A, Olsson L, Riggins GJ, Sartore-Bianchi A, Schmidt K, Shih IM, Oba-Shinjo SM, Siena S, Theodorescu D, Tie J, Harkins TT, Veronese S, Wang TL, Weingart JD, Wolfgang CL, Wood LD, Xing D, Hruban RH, Wu J, Allen PJ, Schmidt CM, Choti MA, Velculescu VE, Kinzler KW, Vogelstein B, Papadopoulos N and Diaz LA Jr. Detection of circulating tumor DNA in early- and late-stage human malignancies. Sci Transl Med 2014; 6: 224ra224.

[12] Kirk GD, Lesi OA, Mendy M, Szymanska K, Whittle H, Goedert JJ, Hainaut P and Montesano R. 249(ser) TP53 mutation in plasma DNA, hepatitis B viral infection, and risk of hepatocellular carcinoma. Oncogene 2005; 24: 5858-5867.

[13] Wong IH, Lo YM, Zhang J, Liew CT, Ng MH, Wong N, Lai PB, Lau WY, Hjelm NM and Johnson PJ. Detection of aberrant p16 methylation in the plasma and serum of liver cancer patients. Cancer Res 1999; 59: 71-73.

[14] Diehl F, Schmidt K, Choti MA, Romans K, Goodman S, Li M, Thornton K, Agrawal N, Sokoll L, Szabo SA, Kinzler KW, Vogelstein B and Diaz LA Jr. Circulating mutant DNA to assess tumor dynamics. Nat Med 2008; 14: 985-990.

[15] Vogelstein B, Papadopoulos N, Velculescu VE, Zhou S, Diaz LA Jr and Kinzler KW. Cancer genome landscapes. Science 2013; 339: 1546-1558.

[16] Roschewski M, Dunleavy K, Pittaluga S, Moorhead M, Pepin F, Kong K, Shovlin M, Jaffe ES, Staudt LM, Lai C, Steinberg SM, Chen CC, Zheng J, Willis TD, Faham M and Wilson WH. Circulating tumour DNA and CT monitoring in patients with untreated diffuse large B-cell lymphoma: a correlative biomarker study. Lancet Oncol 2015; 16: 541-549.

[17] Lv X, Zhao M, Yi Y, Zhang L, Guan Y, Liu T, Yang L, Chen R, Ma J and Yi X. Detection of rare mutations in CtDNA using next generation sequencing. J Vis Exp 2017.

[18] Bailey MH, Tokheim C, Porta-Pardo E, Sengupta S, Bertrand D, Weerasinghe A, Colaprico A, Wendl MC, Kim J, Reardon B, Ng PK, Jeong KJ, Cao S, Wang Z, Gao J, Gao Q, Wang F, Liu EM, Mularoni L, Rubio-Perez C, Nagarajan N, Cortés-Ciriano I, Zhou DC, Liang WW, Hess JM, Yellapantula VD, Tamborero D, Gonzalez-Perez A, Suphavilai C, Ko JY, Khurana E, Park PJ, Van Allen EM, Liang H; MC3 Working Group; Cancer Genome Atlas Research Network, Lawrence MS, Godzik A, Lopez-Bigas N, Stuart J, Wheeler D, Getz G, Chen K, Lazar AJ, Mills GB, Karchin R and Ding L. Comprehensive characterization of cancer driver genes and mutations. Cell 2018; 173: 371-385, e18.

[19] Ma M, Zhu H, Zhang C, Sun X, Gao X and Chen G. "Liquid biopsy"-ctDNA detection with great potential and challenges. Ann Transl Med 2015; 3: 235.

[20] Chen K, Zhang H, Zhang LN, Ju SQ, Qi J, Huang DF, Li F, Wei Q and Zhang J. Value of circulating cell-free DNA in diagnosis of hepatocelluar carcinoma. World J Gastroenterol 2013; 19: 3143-3149.

[21] Huang Z, Hua D, Hu Y, Cheng Z, Zhou X, Xie Q, Wang Q, Wang F, Du X and Zeng Y. Quantitation of plasma circulating DNA using quantitative PCR for the detection of hepatocellular carcinoma. Pathol Oncol Res 2012; 18: 271-276.

[22] Weng W, Feng J, Qin H and Ma Y. Molecular therapy of colorectal cancer: progress and future directions. Int J Cancer 2015; 136: 493-502.

[23] Gouas DA, Shi H, Hautefeuille AH, Ortiz-Cuaran SL, Legros PC, Szymanska KJ, Galy O, Egevad LA, Abedi-Ardekani B, Wiman KG, Hantz O, Caron de Fromentel C, Chemin IA and Hainaut PL. Effects of the TP53 p.R249S mutant on proliferation and clonogenic properties in human hepatocellular carcinoma cell lines: interaction with hepatitis B virus X protein. Carcinogenesis 2010; 31: 1475-1482.

[24] Lereau M, Gouas D, Villar S, Besaratinia A, Hautefeuille A, Berthillon P, Martel-Planche G, Nogueira da Costa A, Ortiz-Cuaran S, Hantz O, Pfeifer GP, Hainaut P and Chemin I. Interactions between hepatitis B virus and aflatoxin B(1): effects on p53 induction in HepaRG cells. J Gen Virol 2012; 93: 640-650.

[25] Hodges C, Kirkland JG and Crabtree GR. The many roles of BAF (mSWI/SNF) and PBAF complexes in cancer. Cold Spring Harb Perspect Med 2016; 6.

[26] Varela I, Tarpey P, Raine K, Huang D, Ong CK, Stephens P, Davies H, Jones D, Lin ML, Teague J, Bignell G, Butler A, Cho J, Dalgliesh GL, Galappaththige D, Greenman C, Hardy C, Jia M, Latimer C, Lau KW, Marshall J, McLaren S, Menzies A, Mudie L, Stebbings L, Largaespada DA, Wessels LF, Richard S, Kahnoski RJ, Anema J, Tuveson DA, Perez-Mancera PA, Mustonen V, Fischer A, Adams DJ, Rust A, Chan-on W, Subimerb C, Dykema K, Furge K, Campbell PJ, Teh BT, Stratton MR and Futreal PA. Exome sequencing identifies frequent mutation of the SWI/SNF complex gene PBRM1 in renal carcinoma. Nature 2011; 469: 539-542.

[27] Mathur R, Alver BH, San Roman AK, Wilson BG, Wang X, Agoston AT, Park PJ, Shivdasani RA and Roberts CW. ARID1A loss impairs enhanc-

er-mediated gene regulation and drives colon cancer in mice. Nat Genet 2017; 49: 296-302.
[28] Isakoff MS, Sansam CG, Tamayo P, Subramanian A, Evans JA, Fillmore CM, Wang X, Biegel JA, Pomeroy SL, Mesirov JP and Roberts CW. Inactivation of the Snf5 tumor suppressor stimulates cell cycle progression and cooperates with p53 loss in oncogenic transformation. Proc Natl Acad Sci U S A 2005; 102: 17745-17750.
[29] Hodges HC, Stanton BZ, Cermakova K, Chang CY, Miller EL, Kirkland JG, Ku WL, Veverka V, Zhao K and Crabtree GR. Dominant-negative SMARCA4 mutants alter the accessibility landscape of tissue-unrestricted enhancers. Nat Struct Mol Biol 2018; 25: 61-72.
[30] Li M, Zhao H, Zhang X, Wood LD, Anders RA, Choti MA, Pawlik TM, Daniel HD, Kannangai R, Offerhaus GJ, Velculescu VE, Wang L, Zhou S, Vogelstein B, Hruban RH, Papadopoulos N, Cai J, Torbenson MS and Kinzler KW. Inactivating mutations of the chromatin remodeling gene ARID2 in hepatocellular carcinoma. Nat Genet 2011; 43: 828-829.
[31] Shain AH and Pollack JR. The spectrum of SWI/SNF mutations, ubiquitous in human cancers. PLoS One 2013; 8: e55119.
[32] Friemel J, Rechsteiner M, Frick L, Bohm F, Struckmann K, Egger M, Moch H, Heikenwalder M and Weber A. Intratumor heterogeneity in hepatocellular carcinoma. Clin Cancer Res 2015; 21: 1951-1961.
[33] Gao Q, Wang XY, Zhou J and Fan J. Multiple carcinogenesis contributes to the heterogeneity of HCC. Nat Rev Gastroenterol Hepatol 2015; 12: 13.
[34] Gao Q, Wang XY, Zhou J and Fan J. Heterogeneity of intermediate-stage HCC necessitates personalized management including surgery. Nat Rev Clin Oncol 2015; 12: 10.
[35] Lu LC, Hsu CH, Hsu C and Cheng AL. Tumor heterogeneity in hepatocellular carcinoma: facing the challenges. Liver Cancer 2016; 5: 128-138.
[36] Jeng KS, Chang CF, Jeng WJ, Sheen IS and Jeng CJ. Heterogeneity of hepatocellular carcinoma contributes to cancer progression. Crit Rev Oncol Hematol 2015; 94: 337-347.
[37] Shlush LI, Zandi S, Itzkovitz S and Schuh AC. Aging, clonal hematopoiesis and preleukemia: not just bad luck? Int J Hematol 2015; 102: 513-522.
[38] Genovese G, Kahler AK, Handsaker RE, Lindberg J, Rose SA, Bakhoum SF, Chambert K, Mick E, Neale BM, Fromer M, Purcell SM, Svantesson O, Landen M, Hoglund M, Lehmann S, Gabriel SB, Moran JL, Lander ES, Sullivan PF, Sklar P, Gronberg H, Hultman CM and McCarroll SA. Clonal hematopoiesis and blood-cancer risk inferred from blood DNA sequence. N Engl J Med 2014; 371: 2477-2487.
[39] Tie J, Wang Y, Tomasetti C, Li L, Springer S, Kinde I, Silliman N, Tacey M, Wong HL, Christie M, Kosmider S, Skinner I, Wong R, Steel M, Tran B, Desai J, Jones I, Haydon A, Hayes T, Price TJ, Strausberg RL, Diaz LA Jr, Papadopoulos N, Kinzler KW, Vogelstein B and Gibbs P. Circulating tumor DNA analysis detects minimal residual disease and predicts recurrence in patients with stage II colon cancer. Sci Transl Med 2016; 8: 346ra392.
[40] Chaudhuri AA, Chabon JJ, Lovejoy AF, Newman AM, Stehr H, Azad TD, Khodadoust MS, Esfahani MS, Liu CL, Zhou L, Scherer F, Kurtz DM, Say C, Carter JN, Merriott DJ, Dudley JC, Binkley MS, Modlin L, Padda SK, Gensheimer MF, West RB, Shrager JB, Neal JW, Wakelee HA, Loo BW Jr, Alizadeh AA and Diehn M. Early detection of molecular residual disease in localized lung cancer by circulating tumor DNA profiling. Cancer Discov 2017; 7: 1394-1403.
[41] Garcia-Murillas I, Schiavon G, Weigelt B, Ng C, Hrebien S, Cutts RJ, Cheang M, Osin P, Nerurkar A, Kozarewa I, Garrido JA, Dowsett M, Reis-Filho JS, Smith IE and Turner NC. Mutation tracking in circulating tumor DNA predicts relapse in early breast cancer. Sci Transl Med 2015; 7: 302ra133.
[42] Xu RH, Wei W, Krawczyk M, Wang W, Luo H, Flagg K, Yi S, Shi W, Quan Q, Li K, Zheng L, Zhang H, Caughey BA, Zhao Q, Hou J, Zhang R, Xu Y, Cai H, Li G, Hou R, Zhong Z, Lin D, Fu X, Zhu J, Duan Y, Yu M, Ying B, Zhang W, Wang J, Zhang E, Zhang C, Li O, Guo R, Carter H, Zhu JK, Hao X and Zhang K. Circulating tumour DNA methylation markers for diagnosis and prognosis of hepatocellular carcinoma. Nat Mater 2017; 16: 1155-1161.
[43] Yan J, Fan Z, Wu X, Xu M, Jiang J, Tan C, Wu W, Wei X and Zhou J. Circulating tumor cells are correlated with disease progression and treatment response in an orthotopic hepatocellular carcinoma model. Cytometry A 2015; 87: 1020-1028.

Table S1. Gene information in the sequencing panel

GENESYMBLE	chr	Position in chromsome
ABL1	9	133581767-133589267
ABL2	1	179068461-179068461
ACVR1B	12	52337950-52339663
AKT1	14	105235685-105235685
AKT2	19	40736223-40736223
AKT3	1	243663020-243663020
ALK	2	29415639-29415639
APC	5	112035701-112043201
AR	X	66756373-66763873
ARAF	X	47412998-47420498
ARFRP1	20	62329994-62329994
ARID1A	1	27015021-27022521
ARID1B	6	157091563-157099063
ARID2	12	46116119-46119502
ASXL1	20	30938646-30946146
ATM	11	108086058-108093224
ATR	3	142174353-142176443
ATRX	X	76760355-76760355
AURKA	20	54944444-54944444
AURKB	17	8108048-8108048
AXIN1	16	337439-337439
AXIN2	17	63524680-63524680
AXL	19	41717607-41725107
B2M	15	44996184-45003684
BAK1	6	33540322-33540322
BAP1	3	52435023-52435023
BARD1	2	215593261-215593261
BCL2	18	60790578-60795857
BCL2L1	20	30252260-30252260
BCL2L11	2	111875799-111878490
BCL2L2	14	23768568-23768607
BCL6	3	187439164-187439164
BCOR	X	39910498-39910498
BCORL1	X	129131663-129139163
BCR	22	23515051-23522551
BLM	15	91253078-91260578
BMPR1A	10	88508895-88516395
BRAF	7	140433811-140433811
BRCA1	17	41196311-41196311
BRCA2	13	32882116-32882820
BRIP1	17	59756546-59760656
BTG1	12	92543947-92547173
BTK	X	100604434-100604872
C11orf30	11	76148568-76152599
C1QA	1	22955617-22962617
C1S	12	7160479-7167979
CARD11	7	2945708-2946271
CASP8	2	202090665-202093653
CBFB	16	67055549-67063049
CBL	11	119074084-119076985
CBLB	3	105377108-105377813
CCND1	11	69448372-69454723
CCND2	12	4375401-4382901
CCND3	6	41902670-41902670
CCNE1	19	30295400-30302900
CD79A	19	42375484-42379766
CD79B	17	62006097-62006097
CDC73	1	193083587-193091087
CDH1	16	68763694-68771194
CDK12	17	37615027-37617738
CDK4	12	58141509-58141509
CDK6	7	92234234-92234234
CDK8	13	26821255-26828755
CDKN1A	6	36636736-36636766
CDKN1B	12	12862801-12870301
CDKN2A	9	21967750-21967750
CDKN2B	9	22002901-22002901
CDKN2C	1	51426866-51428141
CEBPA	19	33790839-33792243
CHD2	15	93436050-93440128
CHD4	12	6684998-6686948
CHEK1	11	125487530-125488265
CHEK2	22	29083730-29083730
CIC	19	42781316-42782370
CREBBP	16	3775054-3775098
CRKL	22	21264213-21271713
CRLF2	X	1314868-1314869
CSF1R	5	149432853-149432853
CTCF	16	67588809-67596309
CTNNA1	5	138081606-138089106
CTNNB1	3	41233441-41240941
CYLD	16	50768460-50768528
DAXX	6	33286334-33286334
DDR1	6	30844360-30844826
DDR2	1	162594727-162602227
DNMT1	19	10244021-10244021
DNMT3A	2	25455829-25457147
DOT1L	19	2159056-2164147
EGFR	7	55079224-55086724
ELAC2	17	12894928-12894928
EML4	2	42388989-42396489
EP300	22	41481113-41488516
EPCAM	2	47588786-47596286
EPHA2	1	16450831-16450831
EPHA3	3	89149173-89156673
EPHA5	4	66185280-66189831
EPHB1	3	134506598-134514098

EPHB2	1	23029830-23037330	GID4	17	17935110-17942192
EPHB6	7	142545291-142552791	GNA11	19	3086907-3094407
EPOR	19	11487880-11487880	GNA13	17	63005406-63007094
ERBB2	17	37836892-37840847	GNAQ	9	80335188-80335188
ERBB3	12	56466308-56466391	GNAS	20	57407294-57414794
ERBB4	2	212240441-212240441	GPR124	8	37646900-37654400
ERCC2	19	45854648-45854778	GRIN2A	16	9847264-9847264
ERCC3	2	128014865-128014865	GRM3	7	86265729-86273229
ERG	21	39739182-39739182	GSK3B	3	119540799-119540799
ESR1	6	152004130-152011630	H3F3A	1	226242907-226250407
ETV6	12	11795287-11802787	HDAC1	1	32751766-32757707
EWSR1	22	29656497-29656602	HDAC4	2	239969863-239969863
EXT1	8	118811601-118811601	HGF	7	81331443-81331443
EXT2	11	44109598-44110246	HIF1A	14	62154618-62156839
EZH2	7	148504463-148504737	HIST1H3B	6	26031816-26031877
FAM123B	X	63404996-63409758	HNF1A	12	121409048-121410095
FAM46C	1	118141103-118147408	HRAS	11	532241-532241
FANCA	16	89803958-89804211	HSD17B3	9	98997588-98997741
FANCC	9	97861335-97861335	HSD3B2	1	119950053-119950242
FANCD2	3	10060612-10065241	HSP90AA1	14	102547074-102547074
FANCE	6	35412637-35420137	IDH1	2	209100952-209100952
FANCF	11	22644078-22646231	IDH2	15	90627209-90627209
FANCG	9	35073834-35073834	IGF1R	15	99185260-99192760
FANCL	2	58386377-58386377	IGF2	11	2150346-2150346
FBXW7	4	153242409-153242409	IKBKE	1	206637783-206643585
FCGR2A	1	161467704-161475204	IKZF1	7	50336877-50344377
FCGR2B	1	161625404-161632904	IL7R	5	35849476-35856976
FCGR3A	1	161511548-161511548	INHBA	7	41728600-41729247
FGF10	5	44305096-44305294	IRF4	6	384238-391738
FGF14	13	102373204-102375180	IRS2	13	110406183-110406183
FGF19	11	69513005-69513005	JAK1	1	65298905-65298915
FGF23	12	4477392-4479508	JAK2	9	4977744-4985244
FGF3	11	69624735-69625072	JAK3	19	17935590-17935590
FGF4	11	69587796-69588076	JUN	1	59246462-59246462
FGF6	12	4543307-4543360	KAT6A	8	41786996-41789722
FGFR1	8	38268655-38268655	KDM5A	12	389222-394621
FGFR2	10	123237843-123237843	KDM5C	X	53220502-53220502
FGFR3	4	1787538-1795038	KDM6A	X	44724922-44732422
FGFR4	5	176506420-176509050	KDR	4	55944425-55946107
FH	1	241660856-241660856	KEAP1	19	10596795-10596795
FLCN	17	17115525-17115525	KIF1B	1	10263263-10270763
FLT1	13	28874482-28877303	KIF5B	10	32297937-32297937
FLT3	13	28577410-28577410	KIT	4	55516594-55524094
FLT4	5	180028505-180030191	KLF4	9	110247132-110247132
FOXL2	3	138672830-138673482	KLHL6	3	183205318-183209714
FUBP1	1	78413590-78414450	KRAS	12	25358179-25358179
GAB2	11	77926335-77926335	LMO1	11	8245850-8245850
GATA1	X	48637481-48644981	LYN	8	56784885-56792385
GATA2	3	128198264-128198264	MAP2K1	15	66671710-66679210
GATA3	10	8089166-8092412	MAP2K2	19	4090318-4090318

MAP2K4	17	11916634-11924134	PAX5	9	36838530-36840556
MAP3K1	5	56103399-56110899	PBRM1	3	52579367-52579367
MAPK1	22	22113945-22118529	PCM1	8	17772865-17780365
MAPK3	16	30125425-30125425	PDGFRA	4	55087763-55095263
MAX	14	65529373-65541841	PDGFRB	5	149493401-149493401
MC1R	16	89976786-89976996	PDK1	2	173413278-173420778
MCL1	1	150547026-150547026	PHF6	X	133499841-133507341
MDM2	12	69194470-69201970	PIK3C2B	1	204391757-204393979
MDM4	1	204478006-204485506	PIK3CA	3	178858810-178866310
MED12	X	70338981-70339220	PIK3CB	3	138371539-138371539
MEF2B	19	19256375-19256375	PIK3CG	7	106498423-106505923
MEN1	11	64570985-64570985	PIK3R1	5	67504083-67511583
MET	7	116304958-116312458	PIK3R2	19	18256515-18256550
MITF	3	69781085-69788585	PML	15	74294463-74315166
MLH1	3	37027340-37027356	PMS1	2	190641310-190647145
MLH3	14	75480466-75480466	PMS2	7	6012869-6012869
MLL	11	118299704-118303855	PRDM1	6	106526694-106534194
MLL2	12	49420129-49421105	PRKAA1	5	40759480-40762879
MLL3	7	151832009-151832009	PRKAR1A	17	66500609-66501042
MPL	1	43795974-43803474	PRKDC	8	48685668-48686733
MRE11A	11	94150465-94153290	PRPF40B	12	50009696-50009902
MS4A1	11	60215781-60223281	PRSS8	16	31142753-31143329
MSH2	2	47622705-47630205	PSMB1	6	170844203-170844203
MSH6	2	48002720-48010220	PSMB5	14	23495059-23495059
MSR1	8	15965386-15967593	PTCH1	9	98205263-98205263
MTOR	1	11167438-11167541	PTCH2	1	45285515-45286360
MUTYH	1	45794913-45794913	PTEN	10	89615694-89618917
MYC	8	128740814-128748314	PTPN11	12	112854943-112856535
MYCL1	1	40361095-40363043	PTPRD	9	8314245-8314245
MYCN	2	16073182-16080019	RAC1	7	6406625-6414125
NBN	8	90945563-90945563	RAD50	5	131886714-131892615
NCOR1	17	15933407-15933407	RAD51	15	40979826-40979877
NF1	17	29414444-29421367	RAD51C	17	56776916-56780554
NF2	22	29992044-29999544	RAF1	3	12625099-12625099
NFE2L2	2	178095030-178095030	RARA	17	38457922-38458161
NFKBIA	14	35870715-35870715	RB1	13	48870382-48870648
NKX2-1	14	36985601-36985601	RET	10	43565016-43572516
NOTCH1	9	139388895-139388895	RHEB	7	151163097-151163097
NOTCH2	1	120454175-120454175	RICTOR	5	38938021-38942405
NOTCH3	19	15270443-15270443	RNASEL	1	182542768-182542768
NOTCH4	6	32165463-32166195	RNF43	17	56437063-56437507
NPM1	5	170807207-170813659	ROS1	6	117609529-117609654
NRAS	1	115247084-115250671	RPS14	5	149823791-149823791
NSD1	5	176552579-176553332	RPS6KB1	17	57977806-57987920
NTRK1	1	156778041-156778992	RPTOR	17	78511124-78518624
NTRK2	9	87275965-87277094	RUNX1	21	36160097-36164431
NTRK3	15	88419987-88420165	RUNX1T1	8	92967194-92972469
NUP93	16	56756516-56763415	SDHAF2	11	61204964-61205094
PAK3	X	110180012-110187512	SDHB	1	17345923-17349100
PALB2	16	23615139-23619182	SDHC	1	161287262-161293401

SDHD	11	111955874-111956018
SETBP1	18	42252637-42253362
SETD2	3	47057897-47057897
SF1	11	64535687-64535758
SF3B1	2	198256697-198256697
SLIT2	4	20247734-20255234
SMAD2	18	45359465-45359465
SMAD3	15	67350694-67358194
SMAD4	18	48549082-48556582
SMARCA4	19	11064097-11064307
SMARCB1	22	24121649-24122543
SMO	7	128821212-128828712
SOCS1	16	11348273-11348699
SOX10	22	38368318-38368318
SOX2	3	181422211-181429711
SOX9	17	70109660-70110344
SPEN	1	16166858-16174358
SPOP	17	47676245-47676245
SPRY4	5	141689991-141693773
SRC	20	35965587-35967056
SRD5A2	2	31749655-31751265
SRSF2	17	74730381-74730842
STAG2	X	123086974-123088055
STAT4	2	191894301-191894301
STK11	19	1198297-1205797
SUFU	10	104256218-104262354
SUZ12	17	30256543-30264043
SYK	9	93556511-93556706
TAF1	X	70578613-70586113
TBX3	12	115108058-115108058
TERT	5	1253281-1253842
TET2	4	106059531-106060341
TFG	3	100420633-100420674
TGFBR2	3	30640493-30647993
TMEM127	2	96915945-96919545
TNFAIP3	6	138180824-138186293
TNFRSF14	1	2480304-2481358
TOP1	20	39649961-39652406
TOP2A	17	38544772-38545770
TP53	17	7571719-7572926
TRAF7	16	2204141-2204802
TRRAP	7	98475173-98476112
TSC1	9	135766734-135766734
TSC2	16	2090489-2093565
TSHR	14	81414368-81421868
TYR	11	88903539-88911039
U2AF1	21	44513065-44513065
U2AF2	19	56157915-56158953
VEGFA	6	43730445-43737945
VHL	3	10175818-10183318
WISP3	6	112367777-112367870
XPO1	2	61705068-61705349
ZNF217	20	52183609-52183609
ZNF703	8	37545800-37553300
ZRSR2	X	15801073-15803838
MYD88	3	38137439-38143022
PPP2R1A	19	52189802-52226425

Table S2. Quality control information of all samples

sample_ID	sample_type	Clean Data		Mapped Data		Unique Data		Mismatch		Depth	Coverage rate	Capture efficiency
		Total reads	Total Bases	Total mapped reads	Mapping rate	Uniquely mapped reads	Fraction of uniquely mapped reads on target	Effective reads	Mismatch rate			
150000046	Tissue	49250175	3693763125	49030002	99.55%	26641674	73.72%	26764069	0.90%	974	99.96%	61.52%
150000050	Tissue	47564949	3567371175	46777391	98.34%	22062698	70.03%	22138958	0.32%	861	99.99%	56.30%
150000051	Tissue	49646470	3723485250	49431650	99.57%	27080059	72.29%	27192866	0.91%	959	99.96%	60.06%
150000052	Tissue	47156155	3536711625	46903130	99.46%	25500947	73.53%	25600854	0.88%	933	99.97%	61.54%
150000056	Tissue	44173551	3313016325	44002491	99.61%	24345321	72.57%	24432256	0.91%	855	99.96%	60.16%
150000059	Tissue	36185011	2713875825	35762053	98.83%	16139721	66.27%	16202036	0.34%	617	99.99%	53.02%
150000060	Tissue	52453972	3934047900	52238988	99.59%	29861625	72.84%	29963961	0.90%	1015	99.97%	60.18%
150000061	Tissue	40938805	3070410375	40473360	98.86%	14333661	48.41%	14423109	0.85%	691	74.95%	39.39%
150000062	Tissue	39381666	2953624950	38872397	98.71%	17833058	67.56%	17901519	0.33%	685	99.98%	54.13%
150000063	Tissue	32403809	2430285675	31993115	98.73%	14673268	67.61%	14728347	0.33%	564	99.99%	54.14%
150000064	Tissue	39174957	2938121775	38936672	99.39%	14199102	45.48%	14263075	0.88%	612	73.90%	36.27%
150000065	Tissue	41805102	3135382650	41331492	98.87%	19041451	67.62%	19107116	0.33%	729	99.99%	54.26%
150000071	Tissue	48724124	3654309300	48182428	98.89%	22208194	68.60%	22292998	0.30%	863	99.99%	55.12%
150000072	Tissue	49133864	3685039800	48563755	98.84%	21903364	67.39%	21983516	0.33%	855	99.99%	54.14%
150000074	Tissue	27668670	2075150250	27187649	98.26%	8913502	50.12%	9002621	0.85%	495	73.69%	42.00%
150000075	Tissue	58615103	4396132725	58118782	99.15%	32959959	68.11%	33060927	0.93%	1036	99.98%	54.94%
150000079	Tissue	28675228	2150642100	28503754	99.40%	10920895	46.82%	10957960	0.88%	460	73.64%	37.24%
150000081	Tissue	45536792	3415259400	45260909	99.39%	16679589	45.78%	16735763	0.88%	714	74.32%	36.43%
150000112	Tissue	56242909	4218218175	55886207	99.37%	19971540	45.65%	20050351	0.87%	892	75.32%	36.83%
150000115	Tissue	30514573	2288592975	30108290	98.67%	13663158	68.94%	13715891	0.32%	541	99.99%	55.17%
150000121	Tissue	25809715	1935728625	25432580	98.54%	12056292	71.91%	12104479	0.30%	478	99.99%	57.61%
150000122	Tissue	31283708	2346278100	30905036	98.79%	14455105	70.97%	14507960	0.30%	572	99.99%	56.92%
150000123	Tissue	31445542	2358415650	31050634	98.74%	13729576	69.76%	13792598	0.30%	566	99.99%	55.95%
150000124	Tissue	37983153	2848736475	37572754	98.92%	17547323	70.70%	17620876	0.30%	695	99.99%	56.91%
150000125	Tissue	36181315	2713598625	35774073	98.87%	17260307	70.37%	17314942	0.31%	660	99.99%	56.70%
150000126	Tissue	28455857	2134189275	28125206	98.84%	13359667	69.51%	13414965	0.33%	510	99.99%	55.80%
160003524	Plasma	101827575	7637068125	99201665	97.42%	23365001	44.75%	23474178	1.02%	1434	100.00%	47.53%
160003525	Plasma	164446333	12333474975	161519051	98.22%	32071184	36.52%	32209924	0.99%	2032	100.00%	41.71%
160003526	Plasma	90807045	6810528375	88933316	97.94%	22271089	45.80%	22369344	1.00%	1300	100.00%	48.32%
160003527	Plasma	159646803	11973510225	155733992	97.55%	16611654	27.24%	16717478	0.98%	2042	99.98%	43.18%
160003528	Plasma	163524881	12264366075	160180600	97.95%	21663538	32.23%	21779470	0.99%	2151	99.98%	44.40%
160003529	Plasma	168516538	12638740350	165447759	98.18%	37050741	39.64%	37213840	1.00%	2110	99.99%	42.26%
160003530	Plasma	102174920	7663119000	99789693	97.67%	24156488	45.86%	24268083	1.00%	1471	100.00%	48.58%
160003531	Plasma	134317236	10073792700	131266037	97.73%	25426242	36.52%	25550405	1.00%	1649	100.00%	41.45%
160003532	Plasma	178631776	13397383200	174867659	97.89%	34962091	37.46%	35135455	1.01%	2165	99.96%	40.91%
160003533	Plasma	184790116	13859258700	180788810	97.83%	21192329	29.51%	21319470	1.00%	2364	99.97%	43.18%

160003534	Plasma	166993691	12524526825	165442990	99.07%	21044017	28.36%	21161169	0.41%	2013	100.00%	40.68%
160003535	Plasma	183463520	13759764000	182006015	99.21%	23188244	28.25%	23317494	0.41%	2192	99.99%	40.33%
160003536	Plasma	184822033	13861652475	184338263	99.74%	42857409	46.30%	43011059	0.44%	2622	99.99%	47.88%
160003537	Plasma	176962250	13272168750	176392836	99.68%	40157283	45.20%	40314946	0.44%	2452	99.99%	46.77%
160003538	Plasma	211341115	15850583625	209895755	99.32%	26629763	29.79%	26781967	0.41%	2628	100.00%	41.97%
160003539	Plasma	187230990	14042324250	185727196	99.20%	21488953	29.93%	21618645	0.39%	2440	99.99%	43.98%
160003540	Plasma	168883947	12666296025	167437310	99.14%	21066033	30.91%	21188079	0.40%	2231	100.00%	44.58%
160003541	Plasma	162441288	12183096600	161709428	99.55%	30382061	39.86%	30516992	0.42%	2167	99.98%	45.02%
160003542	Plasma	158438481	11882886075	157578605	99.46%	28486789	38.80%	28606149	0.45%	2036	99.98%	43.36%
160003544	Plasma	165203864	12390289800	163323766	98.86%	14099926	24.35%	14179018	0.40%	2097	99.99%	42.83%
150000220	Plasma	54957378	4121803350	54427296	99.04%	21966288	63.31%	22043285	0.39%	1241	99.96%	52.43%
150000220	Plasma	62028116	4652108700	61598413	99.31%	29122046	69.13%	29221865	0.35%	1524	99.94%	57.03%
150000221	Plasma	48075880	3605691000	47693904	99.21%	17575355	66.99%	17636768	0.31%	1170	99.93%	56.51%
150000221	Plasma	58464487	4384836525	57951714	99.12%	28027445	69.13%	28132218	0.34%	1429	99.94%	56.74%
150000222	Plasma	56367223	4227541725	55936247	99.24%	26624769	69.92%	26745391	0.34%	1397	99.93%	57.56%
150000223	Plasma	64607763	4845582225	64334011	99.58%	25380158	62.72%	25470210	0.24%	1485	99.91%	53.37%
150000223	Plasma	86014211	6451065825	85660846	99.59%	32126537	65.04%	32273997	0.21%	2085	99.91%	56.28%
150000224	Plasma	72640690	5448051750	72384585	99.65%	27844171	66.01%	27984710	0.20%	1784	99.90%	57.02%
150000224	Plasma	64429077	4832180775	64137278	99.55%	24927059	64.18%	25035101	0.22%	1538	99.90%	55.41%
150000225	Plasma	96265667	7219925025	95845651	99.56%	22918479	38.25%	23021048	0.20%	1589	99.92%	38.32%
150000225	Plasma	72005026	5400376950	71653055	99.51%	26690558	64.30%	26798480	0.25%	1749	99.96%	56.40%
150000226	Plasma	102222612	7666695900	101842799	99.63%	25529120	38.44%	25663824	0.23%	1604	99.94%	36.44%
150000226	Plasma	64430348	4832276100	64120903	99.52%	26730513	65.59%	26832591	0.26%	1544	99.93%	55.63%
150000227	Plasma	64076405	4805730375	63698284	99.41%	15436775	59.46%	15518351	0.21%	1557	99.95%	56.43%
150000227	Plasma	72598854	5444914050	72236578	99.50%	23741845	61.52%	23849030	0.25%	1706	99.92%	54.55%
150000228	Plasma	73855781	5539183575	73490918	99.51%	21502646	61.82%	21600871	0.23%	1789	99.95%	56.25%
150000228	Plasma	67006799	5025509925	66750146	99.62%	27699067	67.74%	27804580	0.23%	1664	99.92%	57.64%
150000229	Plasma	70969849	5322738675	70506722	99.35%	17337165	58.14%	17435668	0.22%	1691	99.95%	55.37%
150000229	Plasma	65166207	4887465525	64891307	99.58%	26857646	65.64%	26966742	0.24%	1571	99.94%	55.96%
150000230	Plasma	77310196	5798264700	76945016	99.53%	21149759	61.81%	21270577	0.21%	1897	99.95%	56.96%
150000230	Plasma	65423227	4906742025	65103723	99.51%	23959348	63.12%	24060629	0.23%	1536	99.96%	54.50%
150000231	Plasma	117104294	8782822050	116833760	99.77%	32369778	44.08%	32507751	0.18%	2045	99.96%	40.54%
150000231	Plasma	83496003	6262200225	83230463	99.68%	29615011	67.81%	29743348	0.19%	2118	99.96%	58.90%
150000232	Plasma	71959156	5396936700	71668992	99.60%	21709878	65.01%	21806491	0.18%	1778	99.96%	57.37%
150000232	Plasma	87973648	6598023600	87680171	99.67%	33912870	67.39%	34035811	0.21%	2185	99.95%	57.66%
150000233	Plasma	86722000	6504150000	86461158	99.70%	21423680	63.13%	21539899	0.16%	2160	99.95%	57.84%
150000233	Plasma	103912070	7793405250	103585025	99.69%	25999889	41.91%	26106637	0.20%	1776	99.98%	39.68%
150000234	Plasma	92439816	6932986200	91976008	99.50%	29205504	67.07%	29334271	0.80%	2380	99.95%	59.77%
150000234	Plasma	121997823	9149836725	121301001	99.43%	41913876	67.22%	42115589	0.81%	3112	99.96%	59.28%
150000235	Plasma	89855630	6739172250	89383872	99.47%	26444246	66.19%	26575810	0.81%	2300	99.94%	59.43%

150000235	Plasma	118419819	8881486425	117670925	99.37%	39776278	65.98%	39955450	0.82%	2961	99.95%	58.05%
150000237	Plasma	120737906	9055342950	120203255	99.56%	33620508	42.52%	33741987	0.27%	2008	99.95%	38.61%
150000237	Plasma	78381503	5878612725	77990529	99.50%	32327930	63.63%	32432796	0.31%	1795	99.92%	53.17%
150000238	Plasma	66227944	4967095800	65816890	99.38%	18354483	58.73%	18426112	0.27%	1467	99.93%	51.42%
150000238	Plasma	54719447	4103958525	54486055	99.57%	18869073	65.09%	18945485	0.24%	1325	99.92%	56.21%
150000240	Plasma	70635394	5297654550	70433331	99.71%	27869190	65.67%	27972747	0.21%	1724	99.96%	56.66%
150000240	Plasma	69320971	5199072825	69077074	99.65%	26964158	63.84%	27066919	0.23%	1655	99.96%	55.43%
150000241	Plasma	80550597	6041294775	80306101	99.70%	31591837	62.32%	31701158	0.23%	1859	99.97%	53.58%
150000241	Plasma	66357805	4976835375	66121891	99.64%	25236888	63.61%	25336072	0.22%	1584	99.95%	55.44%
150000243	Plasma	83783779	6283783425	83386601	99.53%	36178920	68.29%	36319766	0.82%	2112	99.93%	58.51%
150000243	Plasma	72080199	5406014925	71651486	99.41%	32096083	68.55%	32224900	0.83%	1803	99.92%	58.06%
150000244	Plasma	71082920	5331219000	70699471	99.46%	20338632	63.53%	20456695	0.76%	1828	99.94%	59.72%
150000244	Plasma	63815437	4786157775	63318462	99.22%	22161567	61.46%	22248137	0.28%	1470	99.96%	53.47%
150000245	Plasma	91500344	6862525800	91150386	99.62%	37021617	63.60%	37164053	0.25%	2126	99.95%	53.94%
150000245	Plasma	110846314	8313473550	110333855	99.54%	33961265	60.71%	34116759	0.78%	2656	99.97%	55.62%
150000246	Plasma	50150387	3761279025	49873216	99.45%	15125731	63.27%	15189384	0.21%	1216	99.95%	56.28%
150000246	Plasma	87978634	6598397550	87545292	99.51%	19308572	56.18%	19408544	0.19%	2082	99.97%	54.96%
150000247	Plasma	105996913	7949768475	105514268	99.54%	27797566	59.83%	27925772	0.78%	2576	99.96%	56.43%
150000247	Plasma	95108402	7133130150	94569417	99.43%	23775044	57.92%	23894319	0.21%	2276	99.96%	55.57%
150000250	Plasma	59013314	4425998550	58722387	99.51%	19565156	62.82%	19643275	0.23%	1417	99.95%	55.73%
150000250	Plasma	80713801	6053535075	80329963	99.52%	27917664	62.28%	28028373	0.23%	1897	99.96%	54.56%

Table S3. Clinical characteristics of patients with hepatitis and cirrhosis

Characteristics	Hepatitis (n = 10)	Cirrhosis (n = 10)
Age, years		
Median (range)	32 (18-50)	48.5 (31-76)
Gender		
Male	7 (70%)	10 (100%)
Female	3 (30%)	0 (0%)
HBV infection		
Positive	10 (100%)	8 (80%)
Negative	0 (0%)	2 (20%)
AFP, ng/ml		
Median (range)	9.7 (2.9-89.5)	4.1 (1.5-46.9)

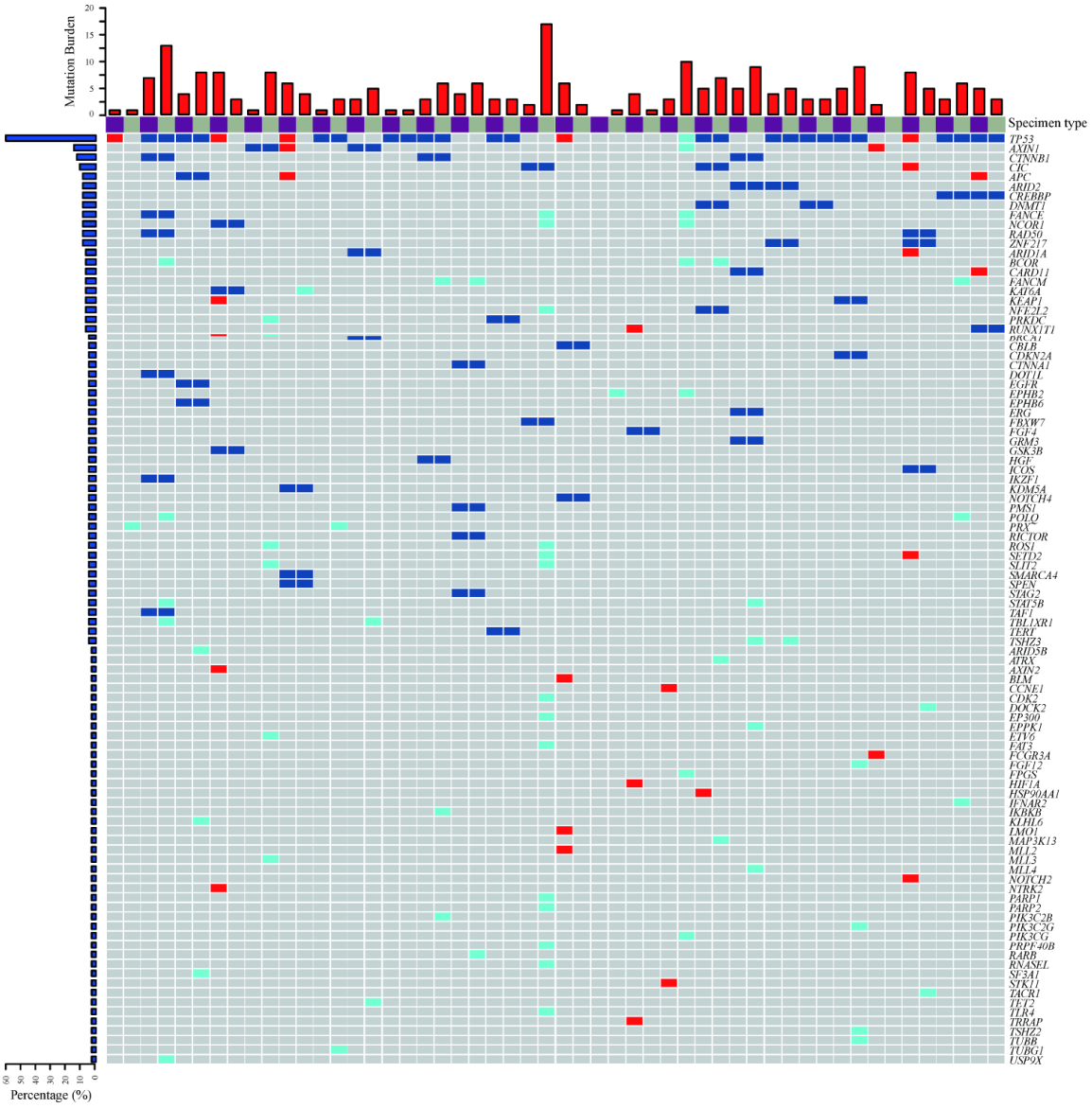

Figure S1. The genomic landscape of matched tissue and plasma samples from HCC patients. The upper bar charts represent the number of mutations in each patient. The left bars show the frequencies of specific altered genes in the total cohort.

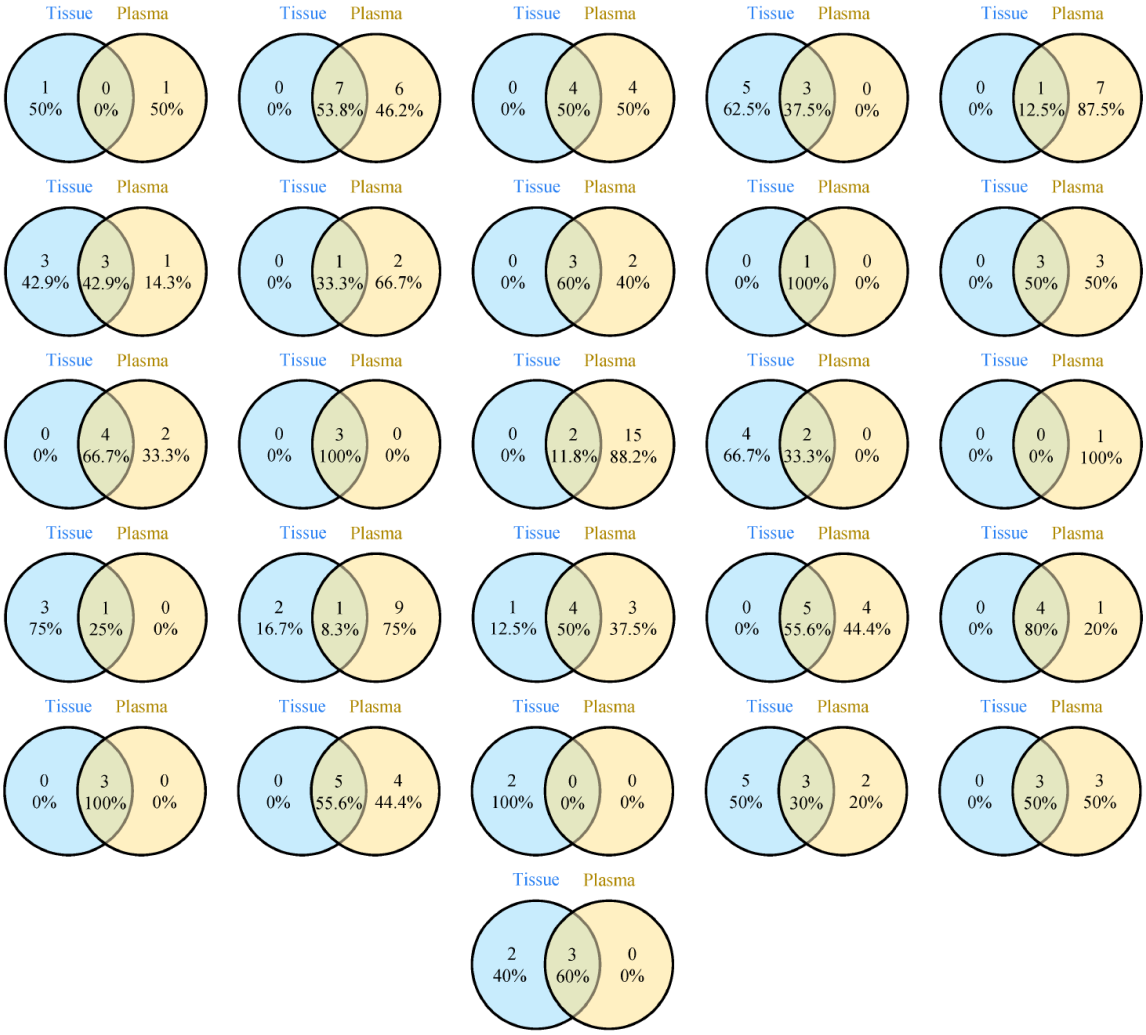

Figure S2. Mutation numbers in matched tissue and plasma samples. Venn diagrams represent the concordance between the mutational spectra of matched tumor tissue and plasma samples for each HCC patient.

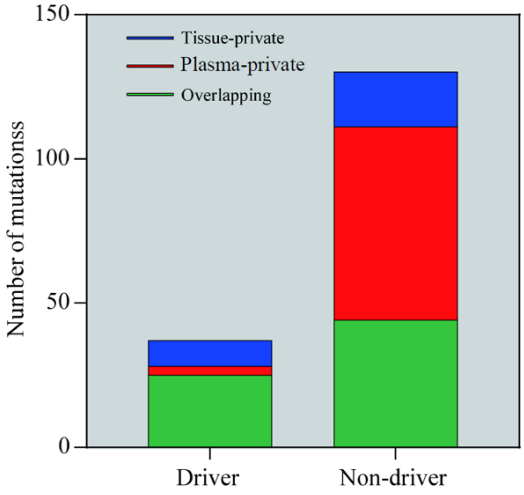

Figure S3. Comparison of concordance rate between driver and non-driver mutations.

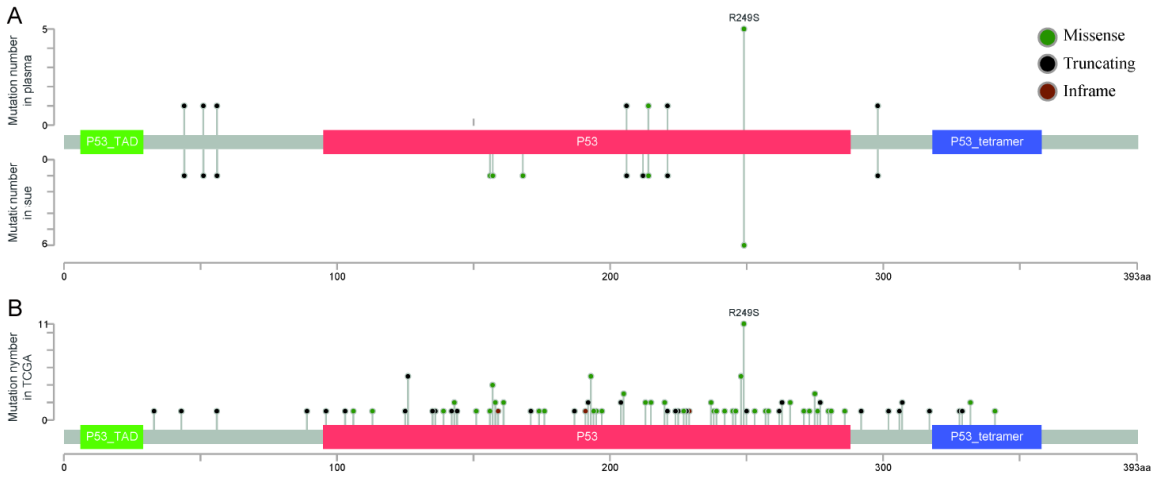

Figure S4. Overview of *TP53* mutations in this study and TCGA database. Lollipop plots of somatic *TP53* mutations identified in the current study (in both plasma and tissue, top section) compare with data obtained from TCGA database (bottom section). Amino acid alterations of R249S are depicted.

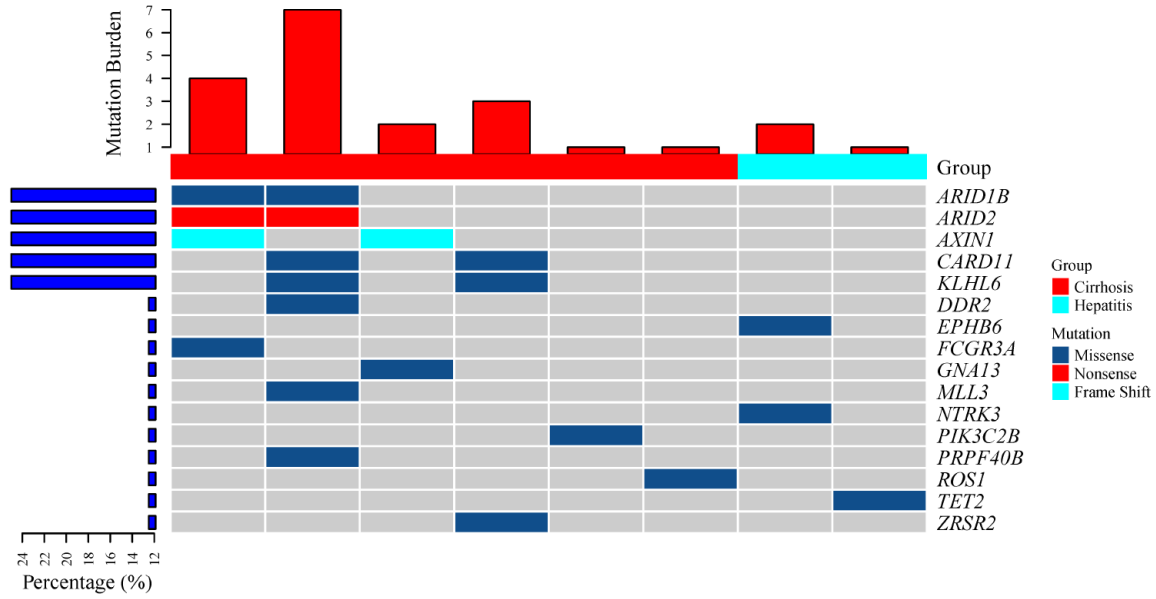

Figure S5. The genomic landscape of cfDNA from hepatitis and cirrhosis patients. The upper bar charts represent the number of mutations in each patient. The left bars show the frequencies of specific altered genes in the total cohort.

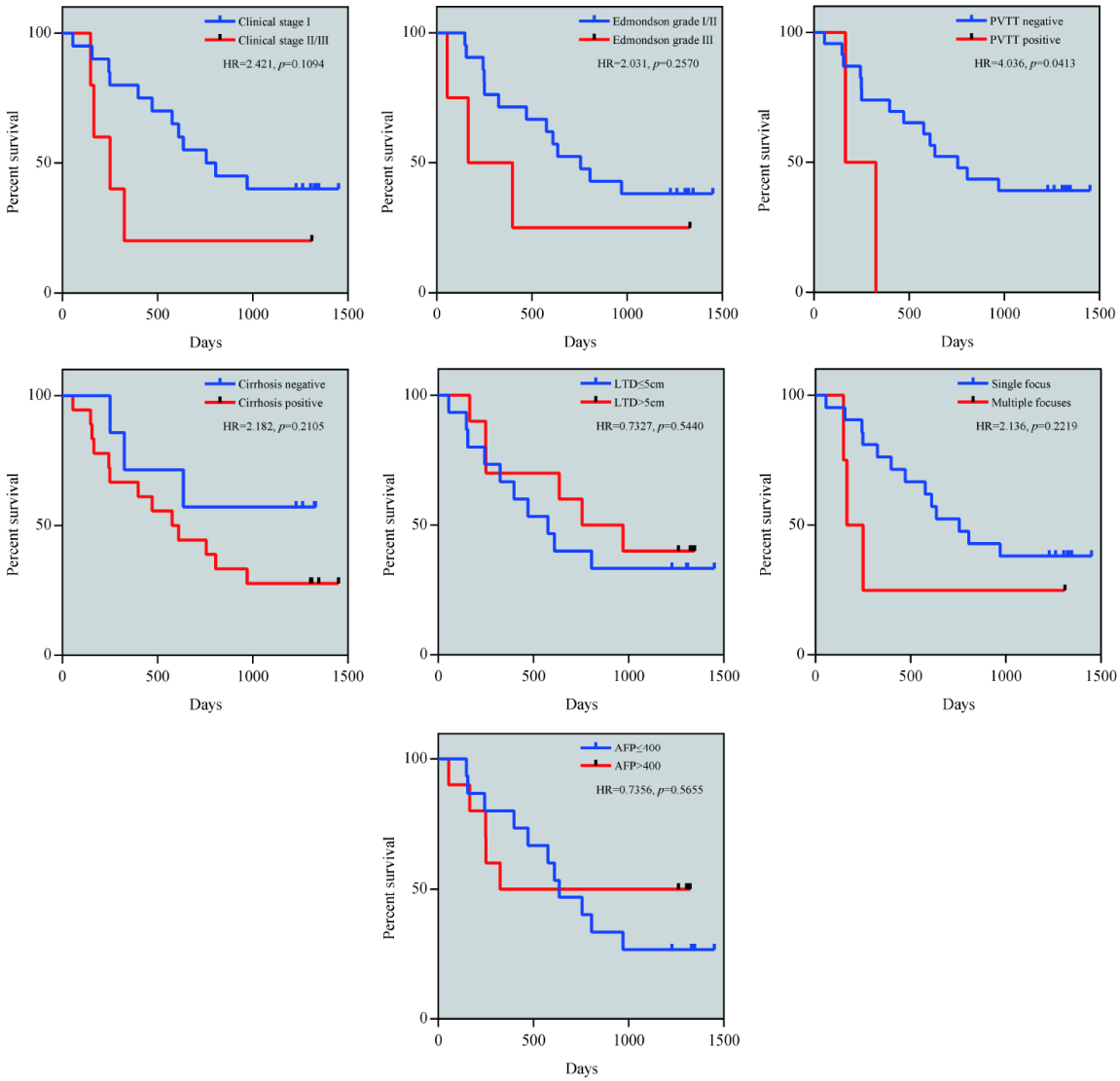

Figure S6. Kaplan-Meier analysis between clinicopathologic risk factors and postoperative survival.